Published in final edited form as:

Cell Rep. 2023 March 28; 42(3): 112198. doi:10.1016/j.celrep.2023.112198.

Tumor suppressor p53 regulates heat shock factor 1 protein degradation in Huntington's disease

Rachel H. Mansky[1,2], **Erin A. Greguske**[1,2], **Dahyun Yu**[1,2], **Nicole Zarate**[1], **Taylor A. Intihar**[1], **Wei Tsai**[1], **Taylor G. Brown**[1], **Mackenzie N. Thayer**[1], **Kompal Kumar**[1], **Rocio Gomez-Pastor**[1,3,*]

[1]Department of Neuroscience, Medical School, University of Minnesota, Minneapolis, MN 55455, USA

[2]These authors contributed equally

[3]Lead contact

SUMMARY

p53 and HSF1 are two major transcription factors involved in cell proliferation and apoptosis, whose dysregulation contributes to cancer and neurodegeneration. Contrary to most cancers, p53 is increased in Huntington's disease (HD) and other neurodegenerative diseases, while HSF1 is decreased. p53 and HSF1 reciprocal regulation has been shown in different contexts, but their connection in neurodegeneration remains understudied. Using cellular and animal models of HD, we show that mutant HTT stabilized p53 by abrogating the interaction between p53 and E3 ligase MDM2. Stabilized p53 promotes protein kinase CK2 alpha prime and E3 ligase FBXW7 transcription, both of which are responsible for HSF1 degradation. Consequently, p53 deletion in striatal neurons of zQ175 HD mice restores HSF1 abundance and decrease HTT aggregation and striatal pathology. Our work shows the mechanism connecting p53 stabilization with HSF1 degradation and pathophysiology in HD and sheds light on the broader molecular differences and commonalities between cancer and neurodegeneration.

Graphical abstract

*Correspondence: rgomezpa@umn.edu.

AUTHOR CONTRIBUTIONS

R.G.P. obtained funding for the study and designed the experiments. Acquisition of data: R.G.P. conducted sip53 and p53-ChIP analyses; R.H.M. conducted Mdm2-p53 immunoprecipitation HTT dot blot experiments; E.A.G. obtained data in mouse models, body weight, synapse density, HSF1 levels, and protein aggregation; D.Y. generated and characterized the p53 cKO mouse in MSNs; N.Z. conducted p53 immunostainings; T.A.I. conducted p53 and HSF1 ChIP and PFT-α experiments; W.T. obtained mRNA data; M.T. and T.G.B. analyzed FOXP1 density; and K.K. obtained p53 transcriptional activity data. Data analyses were performed by R.G.P., R.H.M., E.A.G., D.Y., N.Z., W.T., and M.T.; writing – original draft, R.G.P.; writing – review & editing, R.H.M., E.A.G., D.Y., T.G.B., and N.Z. All authors have read and agreed to the published version of the manuscript.

SUPPLEMENTAL INFORMATION

Supplemental information can be found online at https://doi.org/10.1016/j.celrep.2023.112198.

DECLARATION OF INTERESTS

The authors declare no competing interests.

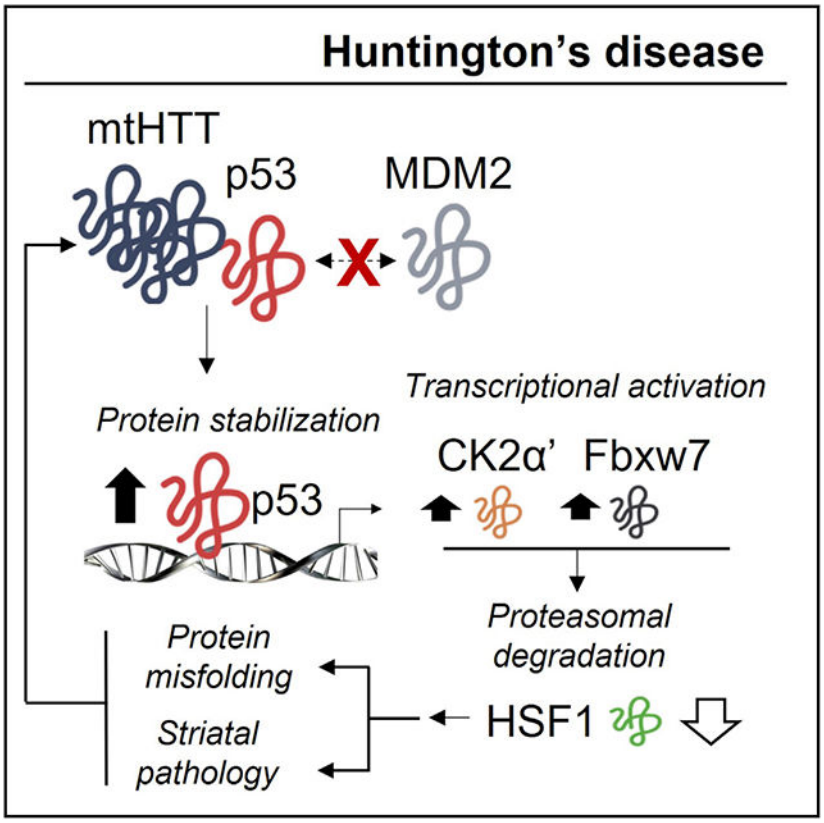

In brief

Huntington's disease (HD) is characterized by a selective degeneration of neurons in the striatum. Mansky et al. propose a mechanism by which these neurons degenerate in HD and show that dysregulation of two major transcription factors involved in apoptosis and stress response cooperate to promote protein aggregation and synaptic dysregulation.

INTRODUCTION

Huntington's disease (HD) is a neurodegenerative disease caused by a polyglutamine (polyQ) expansion in the *HTT* gene that manifests with severe motor and cognitive decline.[1] Medium spiny neurons (MSNs) of the striatum are more susceptible to the misfolding and aggregation of mutant huntingtin (mtHTT) protein than any other cell type, leading to the characteristic striatal degeneration seen in HD and subsequent symptom manifestation.[2] However, cortical degeneration can also be observed in patients with HD at an early symptomatic stage.[3,4] Despite decades of research, the complexity of the molecular mechanisms triggered by mtHTT that lead to striatal pathology has not yet been unraveled.

mtHTT interacts with a large number of proteins and those pathogenic interactions are believed to contribute to the dysregulation of multiple cellular processes that ultimately lead to neuronal dysfunction and death.[5] One major transcription factor reported to interact with mtHTT is tumor suppressor p53,[6,7] a central integrator of various stress signals, such as DNA damage, mitochondrial dysfunction, and apoptosis.[8] Pathological interaction between

mtHTT and p53 contributes to neurodegeneration as reflected in N171-82Q transgenic HD mice systemically lacking p53 (*p53*$^{-/-}$), which provided neuroprotection by restoring transcriptional deficits and improving mitochondrial function.[6] Total levels of p53 are also elevated in the striatum of different mice modeling HD and patients with HD.[6] This correlates with a significantly reduced cancer incidence in HD patients.[9,10] While the detrimental role of p53 in HD is obvious, the mechanism by which p53 levels are induced in HD and how p53 is connected to different cellular processes that are dysregulated in HD remains unknown.

p53 levels are strictly controlled by the E3 ligase MDM2, which promotes p53 ubiquitination and degradation.[11,12] MDM2 inhibition increases p53 levels and activates apoptosis in cancer cells.[13] The MDM2-like p53 binding protein (MDM4) also contributes to the degradation of p53 and the regulation of its transcriptional activity.[14,15] Alternatively, a less-efficient p53 degradation mechanism involves the small chaperone alpha B-crystallin (αB-crys).[16,17] αB-crys$^{-/-}$ cells amass p53 due to the inability of p53 to interact with the E3 ligase Fbx4.[16] αB-crys expression depends on the stress protective heat shock factor 1 (HSF1), a transcription factor essential for the regulation of protein homeostasis and whose protein levels and activity are reduced in HD.[18] Increased p53 and decreased HSF1 protein levels are also observed in Parkinson's disease (PD) and Alzheimer's disease (AD),[19-22] suggesting that these two transcription factors are subject to similar alterations across different neurodegenerative diseases.

HSF1 is progressively degraded in HD by the actions of protein kinase CK2 alpha prime (CK2α′) and the E3 ligase Fbxw7, which phosphorylate and ubiquitylate HSF1, respectively.[23] CK2α′ and Fbxw7 mRNA levels are induced in HD, although the upstream regulator responsible for such alteration is unknown.[23] Contrary to p53, R6/2 HD mice lacking *Hsf1* (*Hsf1*$^{-/-}$) presented mitochondrial abnormalities, increased neuronal mtHTT aggregation, and a shortened lifespan.[24] Conversely, expression of a constitutively active form of HSF1 or attenuation of HSF1 degradation by genetic depletion of CK2α′ resulted in decreased HTT aggregation, restored mitochondrial gene expression, and improved motor behavior and lifespan.[23,25] Reciprocal regulation between p53 and HSF1 has been reported in different contexts, including DNA damage, heat shock, and cancer.[13,17,26-29] These studies suggest that p53 and HSF1 may operate in a unifying stress response pathway under physiological and disease conditions. While alterations in p53 and HSF1 were independently reported in HD, the mechanistic connection between the alteration of these two major transcription factors in HD has not yet been established.

Here, we showed that mtHTT enhanced p53 stabilization by altering the interaction between p53 and MDM2. We showed that accumulation of p53 in MSNs in zQ175 HD mice was associated with enhanced p53 transcriptional activity and HSF1 depletion. Our data demonstrated that p53 controls HSF1 destabilization by regulating the expression of the components of the HSF1 degradation pathway: CK2α′ and Fbxw7. Consequently, zQ175 mice conditionally lacking p53 in MSNs showed increased HSF1 protein levels, decreased HTT aggregation and striatal pathology, increased striatal excitatory synapse density, and ameliorated motor deficits on the pole test. Our findings uncovered an undescribed

molecular pathway that connects mtHTT with the reciprocal dysregulation of p53 and HSF1 and the pathophysiology of HD.

RESULTS

Mutant HTT disrupts p53 and HSF1 protein stabilization

Reciprocal regulation between p53 and HSF1 has been reported in different contexts, but the potential connection in the alteration of these two major transcription factors in HD remains understudied. We first investigated whether HSF1 and p53 proteins were concomitantly altered in the immortalized murine ST*Hdh*$^{Q111/Q111}$ (Q111, HD) striatal cell model compared with the ST*Hdh*$^{Q7/Q7}$ (Q7, control) cells. We found that, while p53 protein levels were increased in Q111 cells, HSF1 levels were decreased (Figures 1A and 1B). Interestingly, mRNA levels for p53 and HSF1 were opposite to that observed for the protein levels (Figure 1C), suggesting possible posttranslational events involved in the alterations of HSF1 and p53 proteins. Depletion of HSF1 in HD is known to be caused by a phosphorylation-dependent proteasome degradation,[23] but the mechanism responsible for increased p53 accumulation in HD remains poorly understood.[30] We hypothesized that increased p53 in HD might be due to increased protein stabilization.

We explored whether the components responsible for regulating p53 protein turnover, such as MDM2, MDM4, and αB-crys, were altered in Q111 cells (Figures 1D and 1E). As expected, protein levels of αB-crys were decreased in the whole-cell extract (WCE) of Q111 cells, mainly due to the degradation of HSF1.[23] The levels of MDM4 were increased in Q111 cells, while MDM2 levels were not significantly altered among the two cell lines. We then investigated whether mtHTT-mediated changes in p53 levels resulted in alterations in protein-protein interactions between p53 and αB-crys, MDM2 and/or MDM4 (Figures 1D and 1F). First, endogenous p53 immunoprecipitation (p53-IP) in Q7 and Q111 cells showed that p53 preferentially co-IP with expanded HTT (Q111), as previously shown[6,7] (Figures 1D and 1F). Similarly, FLAG-IP conducted in 293T cells co-transfected with full-length human HTT containing Q54 (^{fl}HTT(Q54)-FLAG) and human p53-GFP showed enhanced p53 co-IP when compared with ^{fl}HTT(Q23)-FLAG (Figure S1A and S1B). We also observed that, despite αB-crys being reduced in Q111 cells compared with Q7, the presence of HTT-Q111 increased the interaction between p53 and αB-crys (Figures 1D and 1F). On the contrary, the amount of MDM4 pulled down in the p53-IP was similar between Q7 and Q111 when normalized to the total amount in the WCE. These results suggested that increased p53 levels might not be related to decreased interaction with αB-crys or MDM4. However, HTT-Q111 dramatically decreased the interaction between p53 and MDM2 (Figures 1D and 1F).

MDM2 is considered the major E3 ligase responsible for the regulation of p53 degradation and disruption of the MDM2-p53 interaction may result in enhanced levels of p53 in HD. IP analyses in Q7 cells co-expressing human HTT exon 1 containing Q23-GFP or Q74-GFP expansions and human p53-FLAG demonstrated that human p53 interacted with murine MDM2 (Figures 1G and 1H). We also observed that expanded human exon 1 HTT-Q74 co-IP more efficiently with human p53 than exon 1 HTT-Q23, similarly to the human ^{fl}HTT (Figure S1A and S1B) and the HTT and p53 murine proteins (Figure 1D). This

demonstrated that the presence of polyQ-expanded HTT exon 1 is sufficient to interact with p53. In addition, such interaction interfered with p53-MDM2 co-IP (Figures 1G and 1H). Endogenous p53-IP in human striatum samples showed enhanced co-IP between p53 and HTT in HD patients and decreased MDM2 co-IP when compared with control samples (Figures 1I and 1J). Altogether, our data showed that polyQ-expanded HTT enhanced the interaction with p53 and decreased the interaction between MDM2 and p53, which could explain the increased levels of p53 levels in HD, and that such disruption was accompanied with enhanced HSF1 protein destabilization.

Depletion of p53 in HD cells enhanced HSF1 protein levels and DNA binding to target genes

To determine whether increased stabilization of p53 was responsible for HSF1 depletion in HD, we used a silencing RNA (siRNA) targeting p53 (si*p53*) in Q111 cells and observed a significant increase in HSF1 protein levels when compared with cells treated with a non-targeting siRNA (scramble) (Figures 2A and 2B). We also evaluated the impact of knocking out *p53* on HSF1 levels by comparing WT and $p53^{-/-}$ mouse embryonic fibroblasts (MEFs) transiently transfected with Q23-GFP or Q74-GFP (Figures 2C and 2D). No difference in the number of cells containing aggregates was observed when comparing WT and $p53^{-/-}$ cells expressing Q74-GFP (Figures 2C and 2D), as previously shown in $p53^{-/-}$ primary cortical neurons transfected with N171-82Q-HTT.[6] However, levels of HSF1 were largely impacted by the lack of p53. Expression of Q74-GFP in WT MEFs resulted in a depletion of HSF1 protein levels compared with Q23-GFP-expressing cells (Figures 2E and 2F), similar to that observed when comparing Q111 with Q7 cells (Figure 1A). On the contrary, $p53^{-/-}$ MEFs showed similar HSF1 levels when comparing Q23-GFP with Q74-GFP cells and showed a significant increase when comparing $p53^{-/-}$ and WT cells expressing Q74-GFP (Figures 2E and 2F), demonstrating the necessity of p53 to promote HSF1 depletion in polyQ-expanded HTT-expressing cells.

Nuclear and cytoplasmic fractionation of Q7 and Q111 cells revealed a significant depletion of both cytoplasmic and nuclear HSF1 in Q111 cells (Figures 3A-3C), whereas p53 was exclusively found in the nucleus and was enhanced in this fraction in Q111 cells when compared with Q7 cells. si*p53* significantly increased the amount of HSF1 in both the cytoplasm and nucleus of Q111 cells compared with scramble (Figures 3A-3C). However, no significant changes in HSF1 levels were observed in Q7 cells under si*p53* conditions in either cytoplasmic or nuclear fractions. We also found that increased nuclear HSF1 accumulation in Q111 cells under si*p53* conditions restored HSF1 DNA binding to several target genes for which decreased binding had been previously reported in Q111 vs. Q7 cells.[31] HSF1 chromatin immunoprecipitation (ChIP)-PCR in Q7 and Q111 cells validated that 11 out of 13 selected genes selected from the Riva et al.[31] dataset displayed a significant decrease in HSF1 binding in Q111 cells compared with Q7 cells (Figures 3D and 3E), while p53 depletion increased HSF1 binding in 8 of the 11 selected genes (Figures 3F and 3G). Our data also showed that increased HSF1 DNA binding paralleled increased transcriptional activity in several tested genes, including *Hspa1a* (*Hsp70*), *Abt1, Lgals7, Rab11*, and *BDNF* (Figure S2). Altogether, our data showed that p53 silencing in HD cells increased HSF1 nuclear abundance, HSF1 DNA binding, and expression of its target genes.

p53 regulates the transcription of components of the HSF1 degradation pathway in HD

CK2α′ and Fbxw7, components of the HSF1 degradation pathway in HD, are both transcriptionally upregulated in HD[23] but the mechanism responsible for such dysregulation is unknown. Previous research in tumor cells showed p53 directly regulates *Fbxw7* expression via a p53-binding site located in exon 1b of *Fbxw7* that slightly differs from the canonical p53-binding site.[32,33] In addition, whole-genome cartography of human p53 response elements ranked by transactivation potential highlighted several putative p53 response elements in human CK2α′ with moderate functional association.[34] Therefore, we hypothesized that p53 could regulate HSF1 protein levels in HD by controlling the expression of CK2α' (*Csnk2a2*) and *Fbxw7*.

We first determined whether increased levels of p53 in HD were associated with enhanced transcriptional activity. We used the TransAM-p53 ELISA kit to determine the transcriptional activity of p53 in nuclear extracts of Q7 and Q111 cells and found a significant increase in p53 transcriptional activity in the Q111 cells compared with the Q7 (Figures S3A and S3B). These data suggested that stabilized p53 in HD retains its transcriptional activity. We then conducted *in silico* analyses of the promoter and intergenic regions of mouse *Csnk2a2* to search for putative p53-binding sites and found five sequences homologous to a p53 half-binding site: two sequences in the promoter region (nos. 1 and 2), one sequence in exon 1 (no. 3), and two sequences in introns 2 and 9 (nos. 4 and 6) (Figures 4A and 4B). We also found one sequence homologous to a complete p53-binding site in intron 6 (no. 5). We conducted p53 ChIP in Q7 and Q111 cells to determine if p53 binding to the identified sequences in *Csnk2a2* and *Fbxw7* was enhanced in HD. As a positive control we used *Bax*, a p53-dependent target that is induced in HD.[35,36] We found that p53 binding to *Fbxw7* was significantly increased in Q111 cells compared with Q7 cells (percent input relative to IgG) (Figure 4C). Enhanced p53 binding was also observed in the p53-binding sequences identified in the promoter of *Csnk2a2* (nos. 1 and 2) and in the intronic sequence no. 6 (Figure 4C). These data suggested that increased p53 binding to *Fbxw7* and *Csnk2a2* regulatory sequences in HD cells could enhance their transcription, therefore promoting HSF1 degradation. The *Fbxw7* gene generates three different FBXW7 isoforms (α, β, and γ) associated with different functions.[37] FBXW7α is the isoform associated with HSF1 degradation and upregulated in HD.[23,38] We found that silencing *p53* significantly decreased the mRNA and protein levels of FBXW7α and CK2α′ in Q111 cells, which was accompanied by an increase in HSF1 protein levels (Figures 4D-4G). Similar results were obtained when Q111 cells were treated with the p53 inhibitor pifithrin-α (PFT-α) (Figures S3C-S3E), which inhibits p53 transcriptional activity,[39] and in $p53^{-/-}$ MEFs (Figure S3F). Finally, HSF1-ChIP under CK2α′ silencing conditions (Figures S4A-S4D), which we previously showed is sufficient to increase HSF1 levels in HD,[23] showed a similar improvement in HSF1 DNA binding to target genes that was observed under p53 silencing conditions (Figure S4D). We concluded that p53 stabilization contributed to the transcriptional upregulation of components in the HSF1 degradation pathway, which ultimately led to impaired HSF1 DNA binding and enhanced HSF1 degradation in HD.

Conditional deletion of p53 in MSNs of the zQ175 mouse enhanced HSF1 levels and alleviated HTT aggregation

Previous work reported increased p53 levels in the striatum of N171-82Q and R6/2 mouse models of HD and in patients with HD compared with other brain regions.[6,41] Recently, Hyeon et al.[30] showed that p53 is elevated specifically in MSNs in various mouse models of HD and in patients. We confirmed that p53 levels were preferentially elevated in the striatum of symptomatic zQ175 mice, which was accompanied by a decrease in HSF1 and DARPP-32 (dopamine- and cAMP-regulated phosphoprotein of 32 kDa), an MSN marker whose downregulation in HD is associated with striatal pathology[42,43] (Figures 5A, 5B, and S5A-S5D). Immunofluorescence analyses in the striatum also confirmed that p53 was increased in MSNs due to the enhanced colocalization between p53 and the MSN marker Ctip2 (Figures 5C and S5E), while HSF1 protein levels were reduced in the same cell type in zQ175 mice (Figure S5F).

To determine whether elevated p53 in HD MSNs was responsible for HSF1 depletion and striatal degeneration, we created a conditional p53 KO (p53 cKO) mouse model in MSNs by cross-breeding $p53^{fl/fl}$ mice with zQ175 and the MSN reporter line $Gpr88^{Cre/+}$-GFP[44] (Figures 5C-5E). The newly generated $p53^{fl/fl}$:$Gpr88^{Cre/+}$ and zQ175:$p53^{fl/fl}$:$Gpr88^{Cre/+}$ mice robustly reduced p53 levels in the striatum compared with their corresponding control groups $p53^{fl/fl}$ and zQ175:$p53^{fl/fl}$ (Figures 5D, 5E, and S6A). We first evaluated if the newly generated mice altered body weight loss. Lack of p53 in MSNs in zQ175 mice in either heterozygous $^{fl/+}$) or homozygous ($^{fL/fL}$) mice did not alter the characteristic weight loss observed in zQ175 mice when compared with WT mice (Figures S6B-S6D),[23,43] probably due to the peripheral contribution of mtHTT to body weight loss.[45] Nevertheless, p53 cKO in zQ175 mice (zQ175:$p53^{fl/fl}$:$Gpr88^{Cre/+}$) displayed a significant increase in HSF1 levels in the striatum compared with zQ175:$p53^{fl/fl}$, rescuing expression to nearly basal levels of the control $p53^{fl/fl}$ group (Figures 5F, 5G, and S6E). Increased HSF1 levels were also observed in zQ175 mice upon p53 depletion in a heterozygous ($p53^{fl/+}$) background compared with zQ175 mice (Figure S6F). No changes in the levels of the MSN marker FoxP1 were observed across genotypes in either fl/+ or fl/fl backgrounds (Figures 5F, 5H, S6E, and S6F), indicating that enhanced levels of HSF1 were most likely due to a direct increase in HSF1 stabilization rather than an overall impact in neuronal abundance.

Previous studies where the levels and/or activity or HSF1 were increased in cell and mouse models of HD resulted in decreased HTT aggregation due to the role of HSF1 in the regulation of protein homeostasis.[18,23] Lack of p53 in MEFs transfected with Q74-GFP did not show significant differences in the number of cells containing HTT aggregates compared with WT+Q74-GFP-expressing cells despite having increased HSF1 (Figures 2C and 2D). We reasoned that there could be a threshold in the efficacy of HSF1-dependent quality control machinery in decreasing aggregates depending on the HTT concentration (ectopic overexpression vs. endogenous expression). Therefore, we assessed whether conditional deletion of p53 in MSN, and consequently increased HSF1 levels, impacted endogenous HTT aggregation in the striatum of zQ175 mice (Figure 6). Overall, we found a significant decrease in the number of HTT puncta in the striatum of zQ175:$p53^{fl/fl}$:$Gpr88^{Cr0/+}$ mice compared with zQ175:$p53^{fl/fl}$, which was confirmed by immunoblotting (Figures 6A-6C).

Interestingly, when HTT puncta analyses were dissociated between nuclear and non-nuclear aggregates, we found that the non-nuclear aggregates showed a greater depletion in zQ175:p53$^{fl/fl}$:Gpr88$^{Cre/+}$ compared with the nuclear HTT puncta (Figures 6A, 6D, and 6E). It was recently shown that nuclear and cytoplasmic HTT inclusions differ in their structural and molecular complexity, differentially interacting with proteins, lipids, and endomembranes, and implying that different mechanisms may drive the formation and maturation of the different inclusions.[46] Although our data do not allow to identify distinct properties between the nuclear and non-nuclear inclusions, the differential accumulation of cytoplasmic vs. nuclear inclusions in zQ175:p53$^{fl/fl}$:Gpr88$^{Cre/+}$ mice suggests that p53/HSF1-dependent signaling pathways may be preferentially involved in the modulation of cytoplasmic HTT aggregation. On the other hand, no changes in the number of total HTT puncta in the cortex was observed between zQ175:p53$^{fl/fl}$ and zQ175:p53$^{fl/fl}$:Gpr88$^{Cre/+}$ mice (Figure 6F), indicating the selective impact of p53 manipulation in MSN on the HTT aggregation in the striatum.

Conditional deletion of p53 in MSNs alleviated striatal pathology and pole testing deficits

Although the actual toxicity of HTT aggregates in HD remains controversial,[47] there is strong evidence connecting the presence of HTT aggregates to the disruption of striatal synaptic components and synaptic dysfunction.[48-51] The postsynaptic scaffolding protein PSD-95 (*Dlg4*), responsible for anchoring glutamatergic receptors to the postsynaptic membrane and ultimately influencing striatal synaptic density, is among the most dysregulated synaptic components in HD[42,52] and whose expression is regulated by HSF1.[52] In line with these reports, we found that si*p53* in Q111 cells enhanced HSF1 binding to regulatory sequences of *Dlg4* (Figure 3F). We tested whether increased levels of HSF1 in zQ175:p53$^{fl/fl}$:Gpr88$^{Cre/+}$ mice had an impact on PSD-95 levels and striatal synapse density. The striatum receives excitatory input from both the cortex and the thalamus. Loss of thalamo-striatal (T-S) synapses is reported early during disease progression in mouse models of HD and precedes the loss of cortico-striatal (C-S) synapses and several other pathological features, including motor onset.[53,54] T-S synapse density also seems to be preferentially altered by HSF1.[52] Hence, we conducted immunofluorescent staining and colocalization analyses between PSD-95 and VGlut2 (vesicular glutamate transporter 2), used as a marker of thalamic input (Figures 7A, 7B, S7A, and S7B). We first observed that the VGlut2 puncta number was not significantly different between control (p53$^{fl/fl}$) and the HD groups (zQ175:p53$^{fl/fl}$ and zQ175:p53$^{fl/fl}$:Gpr88$^{Cre/+}$) (Figure 7C). However, the PSD-95 puncta number showed a significant reduction in zQ175:p53$^{fl/fl}$ compared with control p53$^{fl/fl}$, and was significantly increased in zQ175:p53$^{fl/fl}$:Gpr88$^{Cre/+}$ compared with zQ175:p53$^{fl/fl}$ (Figure 7D), in concordance with the enhanced levels of HSF1 in those mice. Colocalization between PSD-95 and VGlut2 reflected a similar pattern to that observed for PSD-95, indicating an increase in the T-S synapse density when deleting p53 from MSNs (Figure 7E), potentially leading to the restoration of glutamatergic signaling within the striatum.

DARPP-32 is considered to be a dual glutamate/dopamine-sensitive signaling protein whose transcriptional downregulation in HD-MSN is considered a marker of striatal pathology, although its downregulation is not related with neuronal death.[55-58] We examined

whether conditional depletion of p53 in MSN ameliorated DARPP-32 downregulation in zQ175 mice. DARPP-32 immunostaining showed an intense immunoreactivity in $p53^{fl/fl}$ and $p53^{fl/fl}$:$Gpr88^{Cre/+}$ mice and a robust depletion in zQ175:$p53^{fl/fl}$ and zQ175:$p53^{fl/fl}$:$Gpr88^{Cre/+}$(Figures S7C and S7D). A significant increase in the number of DARPP-32^{+} cells was observed in zQ175 mice lacking p53 in MSN compared with zQ175:$p53^{fl/fl}$, and, although it did not reach WT levels, this increase indicated a partial amelioration of striatal pathology.

Finally, to assess whether restoring p53 levels in the striatum influences mouse behavior, we conducted pole testing, a behavioral task used to assess basal ganglia-related movement disorders in mice, including HD.[59] We assessed the latency to descend the pole in $p53^{fl/+}$, $p53^{fl/+}$:$Gpr88^{Cre/+}$, zQ175:$p53^{fl/+}$, and zQ175:$p53^{fl/+}$:$Gpr88^{Cre/+}$. We used a heterozygous $p53^{fl/+}$ background to better mimic the restoration of p53 levels in the striatum in zQ175 mice, since using a $p53^{fl/+}$ background also increased the levels of HSF1 in this brain region (Figure S6F). We found that zQ175:$p53^{fl/+}$ mice showed a significant decrease in the time to descend the pole compared with $p53^{fl/+}$ and zQ175:$p53^{fl/+}$:$Gpr88^{Cre/+}$ (Figures 7F and 7G). Although increased time to descend the pole is expected upon motor deficits, substantial and significantly decreased times to descend are also associated with motor abnormalities due to mice being unable to turn and descend the pole, falling repeatedly to the cage floor (Figure 7F). We found that zQ175:$p53^{fl/+}$ mice were falling repeatedly from the pole, hence the decreased times to descend. On the contrary, zQ175:$p53^{fl/+}$:$Gpr88^{Cre/+}$ showed a similar time to descend the pole as the control groups and significantly greater than zQ175:$p53^{fl/+}$. These results indicate that conditional depletion of p53 in MSNs of the striatum significantly improved motor behavior assessed on the pole test.

DISCUSSION

Transcription factors p53 and HSF1 control numerous cellular processes and play fundamental roles in physiology and disease.[8,18] In tumor cells, the levels and/or activity of p53 are often reduced and correlate with increased levels and activity of HSF1.[18,60] Contrary to most cancers, increased p53 and decreased HSF1 levels have been shown in different neurodegenerative diseases including PD, AD, and HD.[6,21,61] Interestingly, increased p53 levels in patients with HD are also associated with a significantly reduced cancer incidence.[9,10] Numerous studies have addressed the interconnectivity and reciprocal regulation between these two transcription factors in tumor cells, but studies exploring their potential connection during neurodegeneration were lacking. Here, we show evidence of a mechanistic connection between p53 and HSF1 protein destabilization mediated by mtHTT in HD that ultimately regulates striatal pathology (Figure 7G).

p53 was previously shown to interact with mtHTT and to colocalize with HTT aggregates, but the pathological extent of such interaction was not fully characterized.[6,7] We showed that enhanced binding of mtHTT to p53 disrupted the interaction between p53 and the E3 ligase MDM2, which could contribute to the increased accumulation of p53 in HD. Interestingly, various single-nucleotide polymorphisms in *TP53* that alter binding to MDM2 were reported to influence the age of onset of HD.[62,63] Dissociation between p53 and MDM2 not only stabilizes p53, but it is also necessary for the transactivation of p53.[64] We found that

increased p53 protein levels in HD cells also translated into enhanced p53 transcriptional activity. MDM4 regulates both degradation of p53 and its transcriptional activity,[14,15] but no changes in p53-MDM4 binding were observed in HD cells. Therefore, increased p53 transcriptional activity in HD cells might be preferentially controlled by its interaction with MDM2. Activation of p53 is often associated with the activation of DNA damage response and apoptotic pathways.[65] Therefore, increased stabilization and activation of p53 in HD could contribute to the activation of apoptotic signaling cascades, as shown in transcriptomic analysis in the striatum of an allelic series of HD knockin mice that demonstrated a CAG length-dependent activation of p53 signaling pathways.[66] However, despite increased levels of p53 and the upregulation of genes related to cell death signaling in various mouse models of HD including zQ175 mice, no cell death has been reported in these mouse models of HD even at later stages.[58,66] For this reason, the activation of p53 signaling pathways has been associated with an increased vulnerability of MSNs to degeneration rather than neuronal apoptosis.[66]

We previously showed that HSF1 depletion in HD was caused by the transcriptional upregulation and activation of the CK2α′ kinase and the E3 ligase Fbxw7, which phosphorylate and ubiquitinate HSF1, respectively, signaling HSF1 for proteasomal degradation.[23] Preventing HSF1 degradation by genetic or pharmacological inhibition of CK2α′ in HD cells and mouse models ameliorated HTT aggregation, restored mitochondrial gene expression, and improved synaptic function.[23,58] An open question remained as to which possible upstream mechanism was driving the expression of CK2α′ and Fbxw7 in HD. In tumor cells, p53 directly binds and regulates the expression of *Fbxw7*,[32,33] and decreased expression and/or activity of Fbxw7 in cancer led to increased HSF1 stabilization.[67] Additional evidence showed the presence of putative p53-binding sites in human CK2α'.[34] We demonstrated that p53 directly binds to regulatory elements present in the promoter and intergenic regions of CK2α′ and *Fbxw7*, and enhanced p53 transcriptional activity in HD cells resulted in enhanced transcription of these two genes. We showed that p53-mediated upregulation of CK2α′ and Fbxw7 in HD cells and mice was directly connected to the regulation of HSF1 protein stability. Our findings are supported by previous evidence showing a reciprocal regulation between p53 and HSF1 in different contexts. *Hsf1*$^{-/-}$ MEFs display enhanced levels of p53 in a mechanism connected to the dysregulation of αB-crys,[17] and HSF1 activity is essential for p53 signaling pathways triggered by DNA damage and cancer.[29,68,69] In addition, p53 is required for HSF1 activation and chaperone accumulation after heat shock.[70] This evidence further supports both a physiological and pathological connection between p53 and HSF1, leading to specific transcriptional alterations that influence neuronal pathology associated with HD.

Both HSF1 and p53 are present in all cell types in the body and their functions are essential to ensure a proper response to various stimuli and pathological conditions. We confirmed that p53 levels are primarily elevated in MSNs of the zQ175 mouse model, as shown in other mouse models of HD and in the caudate and putamen of patients with HD,[6,30] coinciding with HSF1 depletion in this cell type. Although there have been discrepancies in the detection of HSF1 depletion in some HD models,[71,72] overwhelming evidence demonstrated decreased HSF1 levels in striatal HD cells and several mouse models of HD, including the knockin Q111 cells, R6/2 and zQ175 mice, in human iPSCs derived from

patients with HD differentiated into MSN-like cells, and in human postmortem striatum from patients with HD.[23,52,73-75] These studies have associated HSF1 depletion in MSNs with the impairment of protein homeostasis and HTT aggregation in HD. Lack of HSF1 also results in mitochondrial abnormalities, transcriptional dysregulation, excitatory synapse impairment, and motor deficits, and when ablated in the R6/2 mouse model it resulted in increased HTT aggregation and reduced lifespan.[24,25,27,52] In contrast, lack of p53 in several models of neurodegenerative diseases, including HD, ameliorated neurodegeneration. For example, lack of p53 in a *C9orf72* mouse model of amyotrophic lateral sclerosis or a mouse model of ataxia SCA1 showed neuroprotection.[76,77] In spinal muscular atrophy (SMA), p53 is a key driver of SMA motor neuron death in both severe and intermediate SMA mouse models, and both genetic and pharmacological inhibition of p53 in SMA models improved motor neuron survival.[78,79] Similarly, lack of p53 in the N171-82Q HD mouse model ameliorated mitochondrial dysfunction and improved motor behavior.[6]

It was suggested that the benefits obtained by systemic deletion of p53 in HD were not related to changes in HTT aggregation since $p53^{KO}$ cortical neurons transfected with N67-104Q-GFP did not alter cytoplasmic or nuclear HTT aggregate formation.[6] We also observed a similar number of cells containing aggregates between WT and $p53^{KO}$ MEFs expressing human HTT exon 1 Q74-GFP, despite the latter having increased HSF1. However, p53 cKO in MSNs in zQ175 mice decreased HTT aggregation in the striatum. A potential explanation for this discrepancy is that, in zQ175 mice, the expression and aggregation of mtHTT is regulated at endogenous levels, while in cell models the ectopic overexpression of polyQ-HTT constructs may elevate HTT aggregation beyond what is physiologically relevant, thereby surpassing the capacity of HSF1-regulated protein quality control systems to deal with such enhanced aggregation. An interesting finding is the differential impact of deleting p53 in MSNs between cytoplasmic and nuclear HTT inclusions. Although p53 cKO in MSNs decreased both cytoplasmic and nuclear inclusions in zQ175 mice, the impact on the nuclear inclusions was much smaller. The structural and molecular complexity of cytoplasmic and nuclear inclusions differ, and the varied proteome found to differentially interact with these inclusions also implies the existence of different mechanisms of formation and regulation between nuclear and cytoplasmic inclusions.[46] Therefore, it is possible that p53/HSF1-dependent signaling pathways are preferentially involved in the formation of cytoplasmic inclusions.

Recently, HSF1 has been shown to be responsible for the regulation of synapse stability by directly regulating the expression of PSD-95 (*Dlg4*).[52] Reduced HSF1 levels in HD are responsible for the downregulation of PSD-95, ultimately altering the formation and maintenance of excitatory synapses. In AD mice, activation of HSF1 increased several synaptic proteins including PSD-95 and the brain-derived neurotrophic factor (BDNF),[80] another HSF1 gene target whose expression is also reduced in HD.[81] We found that p53 silencing in HD cells increased HSF1 DNA binding to several targets including *Dlg4* and *BDNF* and increased their expression. In addition, p53 cKO in MSNs in zQ175 mice resulted in increased PSD-95 puncta. Depletion of PSD-95 preferentially alters T-S synapses in HD.[52] We previously showed that T-S synapses are decreased in $Hsf1^{+/-}$ mice and are rescued in zQ175 mice lacking one allele of CK2α′ with little impact on C-S synapses.[23,52] Our data in zQ175 mice lacking p53 in MSNs also showed significantly

rescued T-S synapses, which is most likely due to an HSF1-dependent increase in PSD-95 levels. Increased T-S synapse density could potentially restore glutamatergic signaling deficits reported in zQ175 mice.[82] In line with this observation, we found a modest but significant increase in the number of DARPP-32+ cells in zQ175:p53$^{fl/fl}$:Gpr88$^{Cre/+}$ compared with zQ175:p53$^{fl/fl}$, indicative of an ameliorated striatal pathology. Since it did not reach WT levels, it is possible that the limited number of DARPP-32+ cells rescued in zQ175:p53$^{fl/fl}$:Gpr88$^{Cre/+}$ mice reflects that a subset of MSNs could be preferentially impacted by the deletion of p53. Due to the lack of neuronal death reported in older zQ175 mice, we attributed the increase of DARPP-32 immunoreactivity to an increase in its transcriptional regulation. DARPP-32 transcriptional regulation is controlled by the BDNF-dependent expression of the early growth response 1[83] and integrates synaptic responses mediated by both dopamine and glutamate.[55] Whether increased expression of DARPP-32 occurs in a specific subset of MSNs in zQ175:p53$^{fl/fl}$:Gpr88$^{Cre/+}$ and whether this is influenced by the HSF1-dependent activation of BDNF expression or by the PSD-95-mediated improvement of glutamatergic synapse density remains unresolved.

Pathological degradation of HSF1 has been reported in other neurodegenerative diseases through various mechanisms. In PD, the E3 ligase NEDD4 is involved in HSF1 degradation while in AD HSF1 is degraded in a mechanism dependent on C/EBP-homologous protein and the activation of the UPR apoptotic pathway.[20] However, increased p53 and CK2, which we showed are upstream modulators of HSF1 degradation in HD, have also been shown in PD and AD.[84-88] In addition, increased FBXW7 has been reported in mouse neurons from PARK2$^{-/-}$ mice, the most frequently mutated gene in hereditary PD,[89] and there is evidence suggesting that FBXW7/SEL-10 facilitates amyloid β formation and could influence pathogenesis of AD.[90] Therefore, although downstream HSF1 degradation components in PD and AD may differ from those reported in HD, it is still possible that a p53-mediated activation of CK2α′ and/or FBXW7 could contribute to HSF1 degradation in these diseases. Future dissecting of the interplay between p53 and HSF1 stabilization in different neurodegenerative diseases could reveal a common molecular mechanism for neuronal dysfunction and neurodegeneration across different diseases and could also shed light into the broader differences and commonalities between cancer and neurodegeneration.

Limitations of the study

Our study proposed a mechanism of neurodegeneration in HD that connects the upregulation of p53 in MSNs with the degradation of HSF1 and the subsequent striatal dysfunction that occurs in mouse models and patients. We also found that p53 preferentially interacts with mtHTT exon 1, interfering with the interaction between p53 and MDM2 and potentially explaining how p53 levels are elevated in HD-MSNs. However, these findings mostly rely on experiments conducted in cell lines overexpressing either HTT exon 1 or full-length HTT with various CAG length repeats, and in mice expressing endogenous levels of mtHTT but with a substantially longer CAG repeat than that seen in patients. A particular limitation exists with experiments overexpressing mtHTT exon 1. Although mtHTT exon 1 is found in patients with HD and is believed to be generated by either mis-splicing of the mtHTT transcript or by proteolysis, its physiological levels are not comparable with those in overexpression experiments. Therefore, although the various models used in our

study are well established in HD research, a question remains as to how these manipulations reproduce the physiological alterations of mtHTT in patients and whether our findings are extrapolatable to the HD-MSN pathophysiology in patients. Further analysis in human lines (i.e., iPSCs) directly derived from patients with HD with endogenous levels of mtHTT or humanized HD mouse models are warranted to fully assess the relevance of HTT levels, CAG size and HTT exon 1 fragments in the connection between p53 and HSF1 in HD.

STAR★METHODS

RESOURCE AVAILABILITY

Lead contact—Further information and requests for resources and reagents should be directed to the lead contact, Dr. Rocio Gomez-Pastor (rgomezpa@umn.edu).

Materials availability—This study did not generate new unique reagents.

Data and code availability

- All data generated in this study is presented in the current manuscript.
- No new datasets or code were generated.
- Any additional information required to reanalyze the data reported in this paper is available from the lead contact upon request.

EXPERIMENTAL MODEL AND SUBJECT DETAILS

Cell lines—Mammalian cell lines used in this study were the mouse-derived striatal cells STHdh$^{Q7/Q7}$ (RRID:CVCL_M590) and STHdh$^{Q111/Q111}$ (RRID:CVCL_M591) (Coriell Cell Repositories). These cells are derived from a knock-in HD mouse model (Htt^{Q111}) expressing full length HTT containing a chimeric mouse/human exon1. No sex information is available from Coriell Cell Repositories for these cells. Cells were grown at 33°C in Dulbecco's modified Eagle's medium (DMEM, Genesee) supplemented with 10% fetal bovine serum (FBS), 100 U ml^{-1} penicillin/streptomycin and 100 μg ml^{-1} G418 (Gibco), as previously described (11). p53$^{-/-}$ MEFs (a gift from Dr. Kirsch at Duke University), carrying a Lox-Stop-Lox (LSL) termination sequence with the K-ras G12D point mutation, were maintained in DMEM supplemented with 10% (FBS), 0.1mM nonessential amino acids, 100Uml^{-1} penicillin/streptomycin, and 55 μM 2-mercaptoethanol and grown at 37°C.

Mouse lines—We used a full-length heterozygous knock-in mouse model of HD known as zQ175 on the C57BL/6J background (#027410, RRI-D:IMSR_JAX:000664).[43] Sperm from HSF1$^{-/-}$ mice (B6N(Cg)-Hsf1$^{tm1(KOMP)Vlcg}$/JMmucd) mice was obtained from the Mutant Mouse Resource and Research Center (University of California, Davis; Davis, CA, USA) (Stock No. 048101-UCD) and generated by the Knockout Mouse Phenotyping Program (KOMP^2). *In vitro* fertilization using C57BL/6N females was conducted at the Mouse Genetics laboratory at University of Minnesota. *Hsf1*$^{-/-: tm1}$ mice were crossbred with CMV-CRE mice (B6.C-Tg(CMV-cre)1Cgn/J, RRID:IMSR_JAX:006054) to delete the Neomycin cassette flanked by loxP sites (*Hsf1*$^{-/-: tm1.1:CRE}$). The *Hsf1*$^{-/-: tm1.1:CRE}$ line was crossed with C57BL/6N to remove the CRE gene (*Hsf1*$^{-/-: tm1.1}$, referenced as

Hsf1$^{-/-}$ in this study). p53$^{fl/fl}$ mice (B6.129P2-*Trp53*^{tm1Brn}/J, RRID:IMSR_JAX:008462) carry a floxed conditional allele of p53 and have normal p53 activity in the absence of Cre recombinase (a gift from Dr. Michael Lee at the University of Minnesota). p53$^{-/-}$ mice (B6;129S2-*Trp53*^{tm1Tyj}/J, RRID:IMSR_JAX:002103.[91] Gpr88$^{Cre/+}$ (G-protein coupled receptor 88) transgenic mice expressing Cre-recombinase and GFP in medium spiny striatal neurons were obtained from Jackson Laboratory (Gpr88$^{tm1.1(cre/GFP)Rpa}$) (#022510, RRID: MGI:6201721). p53 $^{fl/fl}$, Gpr88$^{Cre/+}$, and zQ175 were crossbred for several generations to achieve the desired genotypes for the study. Mixed males and females were used in all analyses. Animals were examined at 6- and 12-month time points. Experimental groups were composed of littermates. All mice were housed under standard SPF conditions and animals had unrestricted access to food and water. Experiments were conducted during the light cycle. All animal care and sacrifice procedures were approved by the University of Minnesota Institutional Animal Care and Use Committee (IACUC) in compliance with the National Institutes of Health guidelines for the care and use of laboratory animals under the approved animal protocol 2007-38316A.

METHOD DETAILS

Immunoprecipitation and immunoblotting—For immunoprecipitation, cell lysates were prepared in cell lysis buffer (20mM HEPES, 5mM MgCl2, 1mM EDTA, 100mM KCl, 0.03% NP-40). Samples were pre-cleared with 50 µl Protein G Dynabeads (Life Technologies) to remove nonspecific interactions for 5 h at 4 C. Beads were removed using a magnet DYNAL (Invitrogen). Cleared samples were incubated overnight at 4 C in the presence of 5 ug anti-p53 antibody (Santa Cruz, D01, RRID: AB_628082) or 5ug mouse IgG anitbody (R&D, AF007, RRID:AB_354520). 50 µl Protein G Dynabeads (Life Technologies) were added to the samples and incubated for 6 h at 4 C. Beads were washed with 0.1M Na-citrate pH 5.3 for 3 times and pull-down antibody was eluted in 50 µl Glycine pH 2. Sample was neutralized with 10 µl 1.5M Tris-HCl pH 8.8 and subjected to immunoblotting. For flag immunoprecipitation, we used EZ view red anti-FLAG M2 affinity gel (F2426) and followed the guidelines provided by Sigma Aldrich.

Sample preparation and immunoblotting conditions were performed as previously described.[23] Protein extracts were prepared in cell lysis buffer (CLB: 25 mM Tris pH 7.4, 150 mM NaCl, 1 mM EDTA, 1% Triton-X100 and 0.1% SDS). Protein samples were separated on 4–20% SDS Criterion TGX Stain-Free gels (BioRad) at 110 V. Proteins were transferred to a nitrocellulose membrane (BioRad 0.2 mm) in Tris–Glycine Buffer (25 nM Tris-Base, 200 mM Glycine) at 25 V for 30 min in Trans Turbo Transfer system (BioRad). The membrane was blocked with 5% non-fat dry milk in TBS containing 0.25% Tween-20 (TBST) for 1 h at room temperature, incubated with primary antibodies in TBST containing 2.5% milk overnight at 4 C, and then washed 3 times for 15 min each in TBST followed by incubation with secondary Amersham ECL HRP Conjugated Antibodies 1:5,000 in TBST containing 2.5% milk (GE Healthcare) for 1 h at room temperature. After washing three times for 15 min each in TBST, bands were detected with SuperSignal Chemiluminiscent substrate (Thermo Scientific) on an ImageQuant LAS 4000.

Dot blot analyses for HTT were conducted in striatum samples solubilized in CLB, pellet fractions were then solubilized in Urea 8M. Primary antibodies are listed in the key resources table and in Table S1. anti-CK2α' (Novus NB100-379, RRID:AB_100000802 and Proteintech 10606-1-AP, RRID:AB_2292447), HTT (Millipore, Mab5374 clone EM48, RRID:AB_10055116), HTT (Abcam, Mabab109115, RID:AB_10863082), HSF1 (Bethyl antibodies A303-176A, RRID:AB_10892628), p53 (Santa Cruz, clone DO1 SC-126, RRID: AB_628082), MDM2 (Santa Cruz sc-965, RRID:AB_627920), MDM4 (Aviva Systems Biology AVARP06007_T100, RRID:AB_841544), aB-crys (Enzo, ADI-SPA-223D, RRID:AB_2039025), FBXW7 (Abcam, Ab109617, RRID:AB_2687519) GAPDH (Santacruz sc-365062, RRID:AB_10847862), Actin (Santa Cruz sc-8432, RRID:AB_626630), H3 (Cell Signaling technology, 9715, RRID:AB_331563), FLAG (Santa Cruz, sc-166355, RRID:AB_2017593), GFP (Santa Cruz, sc-9996, RRID:AB_627695). Protein levels from immunoblots were quantified using ImageJ software. Data was normalized using loading controls GAPDH or Actin.

Cell transfection, RNA isolation and RT-qPCR—For p53 and CK2α′ knock-down, ST*Hdh* cells were transfected with FlexiTube siRNA (5 nmol) from Qiagen using DharmaFECT1 per manufacturer's guidelines. As a negative control, ON-TARGETplus control non-targeting pool siRNA (Dharmacon) was used. Cells were collected 24 h after transfection. RNA was extracted from cells and mouse striatal tissues by using the RNeasy extraction kit (Qiagen) according to the manufacturer's instructions. cDNA was prepared using the Superscript First Strand Synthesis System (Invitrogen). SYBR green based PCR was performed with SYBR mix (Roche). The qPCR amplification was performed using the LightCycler 480 System (Roche). Each sample was tested in triplicate and normalized to GAPDH levels. Primer details are provided in the key resources table and in Table S2. For ectopic expression, cells were transfected using Lipofectamine LTX Reagent (Invitrogen) and following Invitrogen protocol instructions (Invitrogen protocols 25-0946W). Cells were transfected with 10 μg DNA of Q23-GFP (RRID:Addgene_40261) Q74-GFP (RRID:Addgene_40262), p53-FLAG (10838, RRID:Addgene_10838), and harvested 24-48h post-transfection. For cytosolic and nuclear fractionation, cells were fractionated using the NE-PER Extraction Kit (Thermofisher, 78833) as per manufacturer's instructions. RT-qPCR data for all genes was normalized using GAPDH as control.

Chromatin immunoprecipitation—For chromatin immunoprecipitation, cells were grown as described above. Plates were placed on ice and cross-linked with 500 μl Formaldehyde for 5 min at 4 C and quenched with Glycine to a final concentration of 125mM and incubated on ice for 5 min. Cells were lysed in 1ml cell lysis buffer (25mM Tris pH 7.5, 150mM NaCl, 1mM EDTA, 1% Triton X-100, 0.1% SDS) and incubated on ice for 10 min. Lysates were equilibrated in 1ml IP buffer (50mM Tris pH 7.5, 150mM NaCl, 1mM EDTA, 1% Triton X-100) and sonicated three times for 30 s. Samples were centrifuged at 12,000 rpm during 10 min. 5 μg anti-HSF1 (Bethyl antibodies A303-176A, RRID:AB_10892628), 5 μg anti-p53 (Santa-Cruz DO1, RRID: AB_628082) or equal amounts of rabbit and mouse IgG (R&D AF008, RRID:AB_354521 and R&D, AF007, RRID:AB_354520) antibody were use. Dynabeads were added and incubated for 4 h at 4 C. Immunocomplexes were washed, eluted using elution buffer (10mM Tris-HCl, pH

8,1mM EDTA, pH 8,1% SDS), and crosslinking was reversed at 65 C for 12 h. Protein was digested by addition of 5 μl Proteinase K and incubated at 37 C for 2 h. Chromatin was purified using the Qiaquick mini-elute PCR purification kit (Qiagen, 28004) per the manufacturer's instructions. Putative p53-binding sites for Csnk2a2 were identified using https://tfbind.hgc.jp/ and https://molbiol-tools.ca.[92] Data was shown as fold change binding normalized to IgG negative control and % input and relativized to control conditions. See Table S2 for primer details.

Immunofluorescence—Sample preparation was performed as previously described.[23] Mice were perfused intracardially with tris-buffered saline (TBS) (25 mM Tris-base, 135 mM Nacl, 3 mM KCl, pH 7.6) supplemented with 7.5 μM heparin as previously described (McKinstry 2014). Brains were dissected, fixed with 4% PFA ex-vivo in TBS at 4 °C overnight, cryoprotected with 30% sucrose in TBS overnight and embedded in a 2:1 mixture of 30% sucrose in TBS:OCT (Tissue-Tek). Brains were cryo-sectioned at 16 μm using a Leica CM3050S, and stored in a 50/50 solution of TBS and glycerol. Sections were washed and permeabilized in TBS and blocked in 5% normal goat serum (NGS) in TBST (TBS with 0.2% Triton X-100) for 1 h at room temperature. Primary antibodies were diluted in 5% NGS in TBST and sections were incubated overnight at 4°C. Secondary Alexa-fluorophore-conjugated antibodies were added (1:200 in TBST with 5% NGS) for 2 h at room temperature. Slides were mounted in ProLong Gold Antifade Mountant with DAPI (Invitrogen, P36935), and images were either acquired on an epi-fluorescent microscope (Echo Revolve) or confocal microscope (Olympus FV1000). For p53 immunostaining, sucrose-equilibrated brains were paraffin-embedded and sliced at 6 μm. Sections were re-hydrated followed by antigen retrieval (steamed for 30 minutes using Reveal Decloaker, Biocare Medical), membrane permeation (TBST for 10 minutes at room temperature), endogenous peroxidase activity quenching (3% hydrogen peroxide in TBST for 10 minutes at room temperature) and the immunofluorescence protocol.

Coronal brain sections were incubated with primary antibodies described in the key resources table and in Table S1. CK2α' (Proteintech 10606-1-AP; 1:500, Rosemont, IL, USA, RRID:AB_2292447), Ctip2 (Abcam ab18465; 1:500; Waltham, MA, USA, RRID:AB_2064130), DARPP-32 (R&D Systems, MAB4230; 1:1000; Minneapolis, MN, USA, RRID:AB_2169021), HTT (Abcam, ab109115; 1:500, RRID:AB_10863082), HTT (Millipore, clone mEM48 Mab5374; 1:500; Burlington, MA, USA, RRID:AB_11213141), HSF1 (Enzo, ADI-SPA-950F; 1:500; Farmingdale, NY, USA, RRID:AB_11181482), p53 (Novus Biologicals, NB200-10355; 1:200; Centennial, CO, USA, RRID:AB_10001083), GFP (Santa Cruz Biotechnology, SC-9996; 1:200; Dallas, TX, USA, RRID:AB_627695), Ctip2 (Abcam, ab18465; 1:500, RRID:AB_2064130), Foxp1 (Abcam, ab32010; 1:500, RRID:AB_1141518), Cre (Cell Signaling Technology, 15036S; 1:200; Danvers, MA, USA, RRID:AB_2798694), PSD-95 (Thermo Fisher, 51-6900; 1:500; Waltham, MA, USA, RRID:AB_2533914), VGlut2 (Millipore, AB2251-I; 1:1000, RRID:AB_2665454). Then, sections were incubated with their corresponding secondary antibodies (Invitrogen; 1:200; Waltham, MA, USA): goat anti-rabbit, anti-rat, or anti-mouse Alexa 488 (A-11008 RRID:AB_10563748, A-11006 RRID:AB_141373, A-11001 RRID:AB_2534069), goat anti-mouse or anti-rat Alexa 594 (A-11005 RRID:AB_2534073,

A-11007 RRID:AB_10561522), or goat anti-guinea pig, anti-mouse, or anti-rat Alexa 647 (A-21450 RRID:AB_141882, A-21235 RRID:AB_2535804, A-21247 RRID:AB_141778). Finally, sections were mounted on a glass slide with ProLong Gold Antifade Mountant with DAPI (Invitrogen, P36935).

HTT aggregate analyses—EM48 fluorescent images from dorsal striatum (bregma 0.5–1.1 mm) were acquired on a confocal microscope (Olympus FV1000). Confocal stacks (optical section depth of 0.34 mm, 15 sections per stack) in the dorsal striatum were obtained with a 60X objective with a 2x zoom. Maximum projections of optical sections per stack were generated. Puncta analyses were conducted blinded using the Puncta Analyzer Plugin[40] (Durham, NC, USA) on ImageJ, as previously described. A minimum of three slices per animal and three animals per genotype were analyzed. Puncta were calculated as a % relative to the average puncta number of $p53^{fl/fl}$.

p53 transcription factor activity—TransAM p53 Transcription Factor ELISA Kit obtained (Active Motif, 41196) was used to quantify p53 transcriptional activation, according to the manufacturer's instructions. Briefly, nuclear extracts were obtained using the NEN/PER kit (Thermo Scientific, 78833) and were plated on the ELISA with immobilized oligonucleotides containing the p53 consensus binding site. A primary antibody against an epitope of p53 that is exposed upon DNA binding and a secondary antibody conjugated to HRP were added to provide a chemiluminescent readout, and the results were quantified using a spectrophotometer plate reader (spectraMax M series multimode) at 450 nm with reference wavelength of 655 nm.

Synapse density—Sections were washed and permeabilized in TBS. Sections were blocked in 20% normal goat serum (NGS) in TBS for 1 h at room temperature. Primary antibodies were diluted in 10% NGS in TBST (with 0.3% Triton X-100) and sections were incubated overnight at 4°C. Primary antibodies used are as follows: VGLUT2 (Millipore AB2251-I, 1:1000; Burlington, MA, USA), PSD-95 (Thermo Fisher 51-6900, 1:500; Waltham, MA, USA). Secondary Alexa-fluorophore-conjugated antibodies were added (1:200 in TBST with 10% NGS) for 2 h at room temperature. Secondary antibodies used are as follows: goat anti-guinea pig Alexa 488 (1:200) and goat anti-rabbit Alexa 594 (1:200) (Invitrogen; Waltham, MA, USA). Fluorescent images from dorsal striatum (bregma 0.5–1.1 mm) were acquired on a confocal microscope (Olympus FV1000). Confocal stacks (optical section depth 0.34 mm, 15 sections per scan) in the dorsal striatum were performed at 60X magnification with a 4X zoom. Maximum projections of three consecutive optical sections were generated. A minimum of three slices per animal and three animals per genotype were analyzed. Puncta analyses were conducted blinded using the PunctaAnalyzer Plugin (Durham, NC, USA) on ImageJ (RRID:SCR_003070), as previously described.[23,93] Puncta were calculated as a % relative to the average puncta number of $p53^{fl/fl}$.

Pole testing—The pole test is used to estimate motor deficits. The mouse is placed head upward on the top of a vertical rough-surfaced pole (50-cm high and 1-cm wide), the base of the pole is placed in the animal's home cage. The time it takes to orient downward and descend the pole is then recorded. The time to descend the pole is recorded as latency to

descend (seconds). When the animal pauses while descending, the trial is repeated. The test is repeated for 3 trials per animal in each setting and the average time to descend is used for data analysis. Animals were tested at 6 month-old and a total of 3–5 mice/genotype.

QUANTIFICATION AND STATISTICAL ANALYSIS

Protein levels and pixels density from immunoblotting and immunofluorescence images were quantified using ImageJ software. Data are expressed as mean ± SEM, or percentage, analyzed for statistical significance, and displayed by Prism 8 software (GraphPad, San Diego, CA) or Excel software (Microsoft). The statistical information for each experiment can be found in the figure legend. Normal distributions were compared with Student t-test (two-tailed or one-tailed when appropriate), Welch's t -test, or ANOVA with Tukey's post hoc tests for multiple comparisons. The accepted level of significance was $p < 0.05$. When assessing parameters such as HTT puncta, synapse density and cell number in multiple ROIs in different brain slices spanning the striatum region, all collected data was used to determine statistical significance, as previously reported.[54] The numbers of animals or independent experiments (n value) for each experiment were provided in figure legends. No statistical methods were used to predetermine sample sizes, but sample sizes were chosen to be similar to those reported in previous publications.[23,58]

Supplementary Material

Refer to Web version on PubMed Central for supplementary material.

ACKNOWLEDGMENTS

We are grateful to Drs. Michael Lee and Razaul Karim for sharing their expertise on p53 in PD and AD and for kindly providing $p53^{fl/fl}$ mice and other resources, Maha Syed and Joyce Meints for technical assistance, and Jason Mitchell for assistance with confocal microscopy. This research was funded by the National Institute of Neurological Disorders and Stroke (R01NS110694) to R.G.P. and the American Cancer Society and Institutional Research Grant ACS#IRG-16-189-59-IRG107 to R.G.P.

INCLUSION AND DIVERSITY

We support inclusive, diverse, and equitable conduct of research.

REFERENCES

1. Macdonald M, Ambrose CM, Duyao MP, Myers RH, Lin C, Srinidhi L, Barnes G, Taylor SA, James M, Groot N, et al. (1993). A novel gene containing a trinucleotide repeat that is expanded and unstable on Huntington's disease chromosomes. Cell 72, 971–983. 10.1016/0092-8674(93)90585-e. [PubMed: 8458085]
2. DiFiglia M, Sapp E, Chase KO, Davies SW, Bates GP, Vonsattel JP, and Aronin N (1997). Aggregation of huntingtin in neuronal intranuclear inclusions and dystrophic neurites in brain. Science 277, 1990–1993. 10.1126/science.277.5334.1990. [PubMed: 9302293]
3. Rosas HD, Lee SY, Bender AC, Zaleta AK, Vangel M, Yu P, Fischl B, Pappu V, Onorato C, Cha JH, et al. (2010). Altered white matter microstructure in the corpus callosum in Huntington's disease: implications for cortical "disconnection. Neuroimage 49, 2995–3004. 10.1016/j.neuroimage.2009.10.015. [PubMed: 19850138]
4. Tabrizi SJ, Scahill RI, Durr A, Roos RA, Leavitt BR, Jones R, Landwehrmeyer GB, Fox NC, Johnson H, Hicks SL, et al. (2011). Biological and clinical changes in premanifest and early stage

Huntington's disease in the TRACK-HD study: the 12-month longitudinal analysis. Lancet Neurol. 10, 31–42. 10.1016/S1474-4422(10)70276-3. [PubMed: 21130037]

5. Shirasaki DI, Greiner ER, Al-Ramahi I, Gray M, Boontheung P, Geschwind DH, Botas J, Coppola G, Horvath S, Loo JA, and Yang XW (2012). Network organization of the huntingtin proteomic interactome in mammalian brain. Neuron 75, 41–57. 10.1016/j.neuron.2012.05.024. [PubMed: 22794259]
6. Bae BI, Xu H, Igarashi S, Fujimuro M, Agrawal N, Taya Y, Hayward SD, Moran TH, Montell C, Ross CA, et al. (2005). p53 mediates cellular dysfunction and behavioral abnormalities in Huntington's disease. Neuron 47, 29–41. 10.1016/j.neuron.2005.06.005. [PubMed: 15996546]
7. Steffan JS, Kazantsev A, Spasic-Boskovic O, Greenwald M, Zhu YZ, Gohler H, Wanker EE, Bates GP, Housman DE, and Thompson LM (2000). The Huntington's disease protein interacts with p53 and CREB-binding protein and represses transcription. Proc. Natl. Acad. Sci. USA 97, 6763–6768. 10.1073/pnas.100110097. [PubMed: 10823891]
8. Levine AJ (1997). p53, the cellular gatekeeper for growth and division. Cell 88, 323–331. 10.1016/s0092-8674(00)81871-1. [PubMed: 9039259]
9. McNulty P, Pilcher R, Ramesh R, Necuiniate R, Hughes A, Farewell D, Holmans P, and Jones L; REGISTRY Investigators of the European Huntington's Disease Network (2018). Reduced cancer incidence in huntington's disease: analysis in the registry study. J. Huntingtons Dis 7, 209–222. 10.3233/JHD-170263. [PubMed: 30103338]
10. Sørensen SA, Fenger K, and Olsen JH (1999). Significantly lower incidence of cancer among patients with Huntington disease: an apoptotic effect of an expanded polyglutamine tract? Cancer 86, 1342–1346. [PubMed: 10506723]
11. Moll UM, and Petrenko O (2003). The MDM2-p53 interaction. Mol. Cancer Res 1, 1001–1008. [PubMed: 14707283]
12. Fuchs SY, Adler V, Buschmann T, Wu X, and Ronai Z (1998). Mdm2 association with p53 targets its ubiquitination. Oncogene 17, 2543–2547. 10.1038/sj.onc.1202200. [PubMed: 9824166]
13. Oda T, Sekimoto T, Kurashima K, Fujimoto M, Nakai A, and Yamashita T (2018). Acute HSF1 depletion induces cellular senescence through the MDM2-p53-p21 pathway in human diploid fibroblasts. J. Cell Sci 131, jcs210724. 10.1242/jcs.210724. [PubMed: 29632240]
14. Toledo F, and Wahl GM (2007). MDM2 and MDM4: p53 regulators as targets in anticancer therapy. Int. J. Biochem. Cell Biol 39, 1476–1482. 10.1016/j.biocel.2007.03.022. [PubMed: 17499002]
15. Van Alstyne M, Simon CM, Sardi SP, Shihabuddin LS, Mentis GZ, and Pellizzoni L (2018). Dysregulation of Mdm2 and Mdm4 alternative splicing underlies motor neuron death in spinal muscular atrophy. Genes Dev. 32, 1045–1059. 10.1101/gad.316059.118. [PubMed: 30012555]
16. Watanabe G, Kato S, Nakata H, Ishida T, Ohuchi N, and Ishioka C (2009). alphaB-crystallin: a novel p53-target gene required for p53-dependent apoptosis. Cancer Sci. 100, 2368–2375. 10.1111/j.1349-7006.2009.01316.x. [PubMed: 19799611]
17. Jin X, Moskophidis D, Hu Y, Phillips A, and Mivechi NF (2009). Heat shock factor 1 deficiency via its downstream target gene alphaB-crystallin (Hspb5) impairs p53 degradation. J. Cell. Biochem 107, 504–515. 10.1002/jcb.22151. [PubMed: 19343786]
18. Gomez-Pastor R, Burchfiel ET, and Thiele DJ (2018). Regulation of heat shock transcription factors and their roles in physiology and disease. Nat. Rev. Mol. Cell Biol 19, 4–19. 10.1038/nrm.2017.73. [PubMed: 28852220]
19. Jiang YQ, Wang XL, Cao XH, Ye ZY, Li L, and Cai WQ (2013). Increased heat shock transcription factor 1 in the cerebellum reverses the deficiency of Purkinje cells in Alzheimer's disease. Brain Res. 1519, 105–111. 10.1016/j.brainres.2013.04.059. [PubMed: 23665061]
20. Kim E, Wang B, Sastry N, Masliah E, Nelson PT, Cai H, and Liao FF (2016). NEDD4-mediated HSF1 degradation underlies alpha-synucleinopathy. Hum. Mol. Genet 25, 211–222. 10.1093/hmg/ddv445. [PubMed: 26503960]
21. Alves da Costa C, Sunyach C, Pardossi-Piquard R, Sévalle J, Vincent B, Boyer N, Kawarai T, Girardot N, St George-Hyslop P, and Checler F (2006). Presenilin-dependent gamma-secretase-mediated control of p53-associated cell death in Alzheimer's disease. J. Neurosci 26, 6377–6385. 10.1523/JNEUROSCI.0651-06.2006. [PubMed: 16763046]

22. Mogi M, Kondo T, Mizuno Y, and Nagatsu T (2007). p53 protein, interferon-gamma, and NF-kappaB levels are elevated in the parkinsonian brain. Neurosci. Lett 414, 94–97. 10.1016/j.neulet.2006.12.003. [PubMed: 17196747]

23. Gomez-Pastor R, Burchfiel ET, Neef DW, Jaeger AM, Cabiscol E, McKinstry SU, Doss A, Aballay A, Lo DC, Akimov SS, et al. (2017). Abnormal degradation of the neuronal stress-protective transcription factor HSF1 in Huntington's disease. Nat. Commun 8, 14405. 10.1038/ncomms14405. [PubMed: 28194040]

24. Hayashida N, Fujimoto M, Tan K, Prakasam R, Shinkawa T, Li L, Ichikawa H, Takii R, and Nakai A (2010). Heat shock factor 1 ameliorates proteotoxicity in cooperation with the transcription factor NFAT. EMBO J. 29, 3459–3469. 10.1038/emboj.2010.225. [PubMed: 20834230]

25. Fujimoto M, Takaki E, Hayashi T, Kitaura Y, Tanaka Y, Inouye S, and Nakai A (2005). Active HSF1 significantly suppresses polyglutamine aggregate formation in cellular and mouse models. J. Biol. Chem 280, 34908–34916. 10.1074/jbc.M506288200. [PubMed: 16051598]

26. Toma-Jonik A, Widlak W, Korfanty J, Cichon T, Smolarczyk R, Gogler-Piglowska A, Widlak P, and Vydra N (2015). Active heat shock transcription factor 1 supports migration of the melanoma cells via vinculin down-regulation. Cell. Signal 27, 394–401. 10.1016/j.cell-sig.2014.11.029. [PubMed: 25435429]

27. Intihar TA, Martinez EA, and Gomez-Pastor R (2019). Mitochondrial dysfunction in huntington's disease; interplay between HSF1, p53 and PGC-1α transcription factors. Front. Cell. Neurosci 13, 103. 10.3389/fncel.2019.00103. [PubMed: 30941017]

28. Li Q, Feldman RA, Radhakrishnan VM, Carey S, and Martinez JD (2008). Hsf1 is required for the nuclear translocation of p53 tumor suppressor. Neoplasia 10, 1138–1145. 10.1593/neo.08430. [PubMed: 18813348]

29. Logan IR, McNeill HV, Cook S, Lu X, Meek DW, Fuller-Pace FV, Lunec J, and Robson CN (2009). Heat shock factor-1 modulates p53 activity in the transcriptional response to DNA damage. Nucleic Acids Res. 37, 2962–2973. 10.1093/nar/gkp180. [PubMed: 19295133]

30. Hyeon SJ, Park J, Yoo J, Kim SH, Hwang YJ, Kim SC, Liu T, Shim HS, Kim Y, Cho Y, et al. (2021). Dysfunction of X-linked inhibitor of apoptosis protein (XIAP) triggers neuropathological processes via altered p53 activity in Huntington's disease. Prog. Neurobiol 204, 102110. 10.1016/j.pneurobio.2021.102110. [PubMed: 34166773]

31. Riva L, Koeva M, Yildirim F, Pirhaji L, Dinesh D, Mazor T, Duennwald ML, and Fraenkel E (2012). Poly-glutamine expanded huntingtin dramatically alters the genome wide binding of HSF1. J. Huntingtons Dis 1, 33–45. [PubMed: 23293686]

32. Mao JH, Perez-Losada J, Wu D, Delrosario R, Tsunematsu R, Nakayama KI, Brown K, Bryson S, and Balmain A (2004). Fbxw7/Cdc4 is a p53-dependent, haploinsufficient tumour suppressor gene. Nature 432, 775–779. 10.1038/nature03155. [PubMed: 15592418]

33. Kimura T, Gotoh M, Nakamura Y, and Arakawa H (2003). hCDC4b, a regulator of cyclin E, as a direct transcriptional target of p53. Cancer Sci. 94, 431–436. 10.1111/j.1349-7006.2003.tb01460.x. [PubMed: 12824889]

34. Tebaldi T, Zaccara S, Alessandrini F, Bisio A, Ciribilli Y, and Inga A (2015). Whole-genome cartography of p53 response elements ranked on transactivation potential. BMC Genom. 16, 464. 10.1186/s12864-015-1643-9.

35. Teles AVFF, Rosenstock TR, Okuno CS, Lopes GS, Bertoncini CRA, and Smaili SS (2008). Increase in bax expression and apoptosis are associated in Huntington's disease progression. Neurosci. Lett 438, 59–63. 10.1016/j.neulet.2008.03.062. [PubMed: 18468793]

36. Zhang Y, Ona VO, Li M, Drozda M, Dubois-Dauphin M, Przedborski S, Ferrante RJ, and Friedlander RM (2003). Sequential activation of individual caspases, and of alterations in Bcl-2 proapoptotic signals in a mouse model of Huntington's disease. J. Neurochem 87, 1184–1192. 10.1046/j.1471-4159.2003.02105.x. [PubMed: 14622098]

37. Yang Y, Zhou X, Liu X, Song R, Gao Y, and Wang S (2021). Implications of FBXW7 in neurodevelopment and neurodegeneration: molecular mechanisms and therapeutic potential. Front. Cell. Neurosci 15, 736008. 10.3389/fncel.2021.736008. [PubMed: 34512273]

38. Kourtis N, Moubarak RS, Aranda-Orgilles B, Lui K, Aydin IT, Trimarchi T, Darvishian F, Salvaggio C, Zhong J, Bhatt K, et al. (2015). FBXW7 modulates cellular stress response and

metastatic potential through HSF1 post-translational modification. Nat. Cell Biol 17, 322–332. 10.1038/ncb3121. [PubMed: 25720964]

39. Komarov PG, Komarova EA, Kondratov RV, Christov-Tselkov K, Coon JS, Chernov MV, and Gudkov AV (1999). A chemical inhibitor of p53 that protects mice from the side effects of cancer therapy. Science 285, 1733–1737. 10.1126/science.285.5434.1733. [PubMed: 10481009]
40. Farkas M, Hashimoto H, Bi Y, Davuluri RV, Resnick-Silverman L, Manfredi JJ, Debler EW, and McMahon SB (2021). Distinct mechanisms control genome recognition by p53 at its target genes linked to different cell fates. Nat. Commun 12, 484. 10.1038/s41467-020-20783-z. [PubMed: 33473123]
41. Reynolds RH, Petersen MH, Willert CW, Heinrich M, Nymann N, Dall M, Treebak JT, Björkqvist M, Silahtaroglu A, Hasholt L, and Nørremølle A (2018). Perturbations in the p53/miR-34a/SIRT1 pathway in the R6/2 Huntington's disease model. Mol. Cell. Neurosci 88, 118–129. 10.1016/j.mcn.2017.12.009. [PubMed: 29289683]
42. Desplats PA, Kass KE, Gilmartin T, Stanwood GD, Woodward EL, Head SR, Sutcliffe JG, and Thomas EA (2006). Selective deficits in the expression of striatal-enriched mRNAs in Huntington's disease. J. Neurochem 96, 743–757. 10.1111/j.1471-4159.2005.03588.x. [PubMed: 16405510]
43. Menalled LB, Kudwa AE, Miller S, Fitzpatrick J, Watson-Johnson J, Keating N, Ruiz M, Mushlin R, Alosio W, McConnell K, et al. (2012). Comprehensive behavioral and molecular characterization of a new knock-in mouse model of Huntington's disease: zQ175. PLoS One 7, e49838. 10.1371/journal.pone.0049838. [PubMed: 23284626]
44. Naydenov AV, Sepers MD, Swinney K, Raymond LA, Palmiter RD, and Stella N (2014). Genetic rescue of CB1 receptors on medium spiny neurons prevents loss of excitatory striatal synapses but not motor impairment in HD mice. Neurobiol. Dis 71, 140–150. 10.1016/j.nbd.2014.08.009. [PubMed: 25134728]
45. Lakra P, Aditi K, and Agrawal N (2019). Peripheral expression of mutant huntingtin is a critical determinant of weight loss and metabolic disturbances in huntington's disease. Sci. Rep 9, 10127. 10.1038/s41598-019-46470-8. [PubMed: 31300691]
46. Riguet N, Mahul-Mellier AL, Maharjan N, Burtscher J, Croisier M, Knott G, Hastings J, Patin A, Reiterer V, Farhan H, et al. (2021). Nuclear and cytoplasmic huntingtin inclusions exhibit distinct biochemical composition, interactome and ultrastructural properties. Nat. Commun 12, 6579. 10.1038/s41467-021-26684-z. [PubMed: 34772920]
47. Arrasate M, Mitra S, Schweitzer ES, Segal MR, and Finkbeiner S (2004). Inclusion body formation reduces levels of mutant huntingtin and the risk of neuronal death. Nature 431, 805–810. 10.1038/nature02998. [PubMed: 15483602]
48. Tang B, Seredenina T, Coppola G, Kuhn A, Geschwind DH, Luthi-Carter R, and Thomas EA (2011). Gene expression profiling of R6/2 transgenic mice with different CAG repeat lengths reveals genes associated with disease onset and progression in Huntington's disease. Neurobiol. Dis 42, 459–467. 10.1016/j.nbd.2011.02.008. [PubMed: 21334439]
49. Runne H, Régulier E, Kuhn A, Zala D, Gokce O, Perrin V, Sick B, Aebischer P, Déglon N, and Luthi-Carter R (2008). Dysregulation of gene expression in primary neuron models of Huntington's disease shows that polyglutamine-related effects on the striatal transcriptome may not be dependent on brain circuitry. J. Neurosci 28, 9723–9731. 10.1523/JNEUROSCI.3044-08.2008. [PubMed: 18815258]
50. Luthi-Carter R, Strand A, Peters NL, Solano SM, Hollingsworth ZR, Menon AS, Frey AS, Spektor BS, Penney EB, Schilling G, et al. (2000). Decreased expression of striatal signaling genes in a mouse model of Huntington's disease. Hum. Mol. Genet 9, 1259–1271. 10.1093/hmg/9.9.1259. [PubMed: 10814708]
51. Wood TE, Barry J, Yang Z, Cepeda C, Levine MS, and Gray M (2019). Mutant huntingtin reduction in astrocytes slows disease progression in the BACHD conditional Huntington's disease mouse model. Hum. Mol. Genet 28, 487–500. 10.1093/hmg/ddy363. [PubMed: 30312396]
52. Zarate N, Intihar TA, Yu D, Sawyer J, Tsai W, Syed M, Carlson L, and Gomez-Pastor R (2021). Heat shock factor 1 directly regulates postsynaptic scaffolding PSD-95 in aging and huntington's disease and influences striatal synaptic density. Int. J. Mol. Sci 22, 13113. 10.3390/ijms222313113. [PubMed: 34884918]

53. Milnerwood AJ, and Raymond LA (2010). Early synaptic pathophysiology in neurodegeneration: insights from Huntington's disease. Trends Neurosci. 33, 513–523. 10.1016/j.tins.2010.08.002. [PubMed: 20850189]
54. McKinstry SU, Karadeniz YB, Worthington AK, Hayrapetyan VY, Ozlu MI, Serafin-Molina K, Risher WC, Ustunkaya T, Dragatsis I, Zeitlin S, et al. (2014). Huntingtin is required for normal excitatory synapse development in cortical and striatal circuits. J. Neurosci 34, 9455–9472. 10.1523/JNEUROSCI.4699-13.2014. [PubMed: 25009276]
55. Nishi A, Watanabe Y, Higashi H, Tanaka M, Nairn AC, and Greengard P (2005). Glutamate regulation of DARPP-32 phosphorylation in neostriatal neurons involves activation of multiple signaling cascades. Proc. Natl. Acad. Sci. USA 102, 1199–1204. 10.1073/pnas.0409138102. [PubMed: 15657149]
56. Peng Q, Wu B, Jiang M, Jin J, Hou Z, Zheng J, Zhang J, and Duan W (2016). Characterization of behavioral, neuropathological, brain metabolic and key molecular changes in zQ175 knock-in mouse model of huntington's disease. PLoS One 11, e0148839. 10.1371/journal.pone.0148839. [PubMed: 26859386]
57. Deng Y, Wang H, Joni M, Sekhri R, and Reiner A (2021). Progression of basal ganglia pathology in heterozygous Q175 knock-in Huntington's disease mice. J. Comp. Neurol 520, 1327–1371. 10.1002/cne.25023.
58. Yu D, Zarate N, White A, Coates D, Tsai W, Nanclares C, Cuccu F, Yue JS, Brown TG, Mansky RH, et al. (2022). CK2 alpha prime and alpha-synuclein pathogenic functional interaction mediates synaptic dysregulation in Huntington's disease. Acta Neuropathol. Commun 10, 83. 10.1186/s40478-022-01379-8. [PubMed: 35659303]
59. Hickey MA, Kosmalska A, Enayati J, Cohen R, Zeitlin S, Levine MS, and Chesselet MF (2008). Extensive early motor and non-motor behavioral deficits are followed by striatal neuronal loss in knock-in Huntington's disease mice. Neuroscience 157, 280–295. 10.1016/j.neuroscience.2008.08.041. [PubMed: 18805465]
60. Mendillo ML, Santagata S, Koeva M, Bell GW, Hu R, Tamimi RM, Fraenkel E, Ince TA, Whitesell L, and Lindquist S (2012). HSF1 drives a transcriptional program distinct from heat shock to support highly malignant human cancers. Cell 150, 549–562. 10.1016/j.cell.2012.06.031. [PubMed: 22863008]
61. Hooper C, Meimaridou E, Tavassoli M, Melino G, Lovestone S, and Killick R (2007). p53 is upregulated in Alzheimer's disease and induces tau phosphorylation in HEK293a cells. Neurosci. Lett 418, 34–37. 10.1016/j.neulet.2007.03.026. [PubMed: 17399897]
62. Dumont P, Leu JIJ, Della Pietra AC, George DL, and Murphy M (2003). The codon 72 polymorphic variants of p53 have markedly different apoptotic potential. Nat. Genet 33, 357–365. 10.1038/ng1093. [PubMed: 12567188]
63. Chattopadhyay B, Baksi K, Mukhopadhyay S, and Bhattacharyya NP (2005). Modulation of age at onset of Huntington disease patients by variations in TP53 and human caspase activated DNase (hCAD) genes. Neurosci. Lett 374, 81–86. 10.1016/j.neulet.2004.10.018. [PubMed: 15644269]
64. Momand J, Zambetti GP, Olson DC, George D, and Levine AJ (1992). The mdm-2 oncogene product forms a complex with the p53 protein and inhibits p53-mediated transactivation. Cell 69, 1237–1245. 10.1016/0092-8674(92)90644-r. [PubMed: 1535557]
65. Fridman JS, and Lowe SW (2003). Control of apoptosis by p53. Oncogene 22, 9030–9040. 10.1038/sj.onc.1207116. [PubMed: 14663481]
66. Langfelder P, Cantle JP, Chatzopoulou D, Wang N, Gao F, Al-Ramahi I, Lu XH, Ramos EM, El-Zein K, Zhao Y, et al. (2016). Integrated genomics and proteomics define huntingtin CAG length-dependent networks in mice. Nat. Neurosci 19, 623–633. 10.1038/nn.4256. [PubMed: 26900923]
67. Kourtis N, Strikoudis A, and Aifantis I (2015). Emerging roles for the FBXW7 ubiquitin ligase in leukemia and beyond. Curr. Opin. Cell Biol 37, 28–34. 10.1016/j.ceb.2015.09.003. [PubMed: 26426760]
68. Kawamura G, Hattori M, Takamatsu K, Tsukada T, Ninomiya Y, Benjamin I, Sassone-Corsi P, Ozawa T, and Tamaru T (2018). Cooperative interaction among BMAL1, HSF1, and p53 protects mammalian cells from UV stress. Commun. Biol 1, 204. 10.1038/s42003-018-0209-1. [PubMed: 30480104]

69. Toma-Jonik A, Vydra N, Janus P, and Widłak W (2019). Interplay between HSF1 and p53 signaling pathways in cancer initiation and progression: non-oncogene and oncogene addiction. Cell. Oncol 42, 579–589. 10.1007/s13402-019-00452-0.
70. Sharma A, Meena AS, and Bhat MK (2010). Hyperthermia-associated carboplatin resistance: differential role of p53, HSF1 and Hsp70 in hepatoma cells. Cancer Sci. 101, 1186–1193. 10.1111/j.1349-7006.2010.01516.x. [PubMed: 20180806]
71. Gomez-Paredes C, Mason MA, Taxy BA, Papadopoulou AS, Paganetti P, and Bates GP (2021). The heat shock response, determined by QuantiGene multiplex, is impaired in HD mouse models and not caused by HSF1 reduction. Sci. Rep 11, 9117. 10.1038/s41598-021-88715-5. [PubMed: 33907289]
72. Labbadia J, Cunliffe H, Weiss A, Katsyuba E, Sathasivam K, Seredenina T, Woodman B, Moussaoui S, Frentzel S, Luthi-Carter R, et al. (2011). Altered chromatin architecture underlies progressive impairment of the heat shock response in mouse models of Huntington disease. J. Clin. Invest 121, 3306–3319. 10.1172/JCI57413. [PubMed: 21785217]
73. Chafekar SM, and Duennwald ML (2012). Impaired heat shock response in cells expressing full-length polyglutamine-expanded huntingtin. PLoS One 7, e37929. 10.1371/journal.pone.0037929. [PubMed: 22649566]
74. Maheshwari M, Bhutani S, Das A, Mukherjee R, Sharma A, Kino Y, Nukina N, and Jana NR (2014). Dexamethasone induces heat shock response and slows down disease progression in mouse and fly models of Huntington's disease. Hum. Mol. Genet 23, 2737–2751. 10.1093/hmg/ddt667. [PubMed: 24381308]
75. Burchfiel ET, Vihervaara A, Guertin MJ, Gomez-Pastor R, and Thiele DJ (2021). Comparative interactomes of HSF1 in stress and disease reveal a role for CTCF in HSF1-mediated gene regulation. J. Biol. Chem 296, 100097. 10.1074/jbc.RA120.015452. [PubMed: 33208463]
76. Shahbazian MD, Orr HT, and Zoghbi HY (2001). Reduction of Purkinje cell pathology in SCA1 transgenic mice by p53 deletion. Neurobiol. Dis 8, 974–981. 10.1006/nbdi.2001.0444. [PubMed: 11741393]
77. Maor-Nof M, Shipony Z, Lopez-Gonzalez R, Nakayama L, Zhang YJ, Couthouis J, Blum JA, Castruita PA, Linares GR, Ruan K, et al. (2021). p53 is a central regulator driving neurodegeneration caused by C9orf72 poly(PR). Cell 184, 689–708.e20. 10.1016/j.cell.2020.12.025. [PubMed: 33482083]
78. Buettner JM, Sime Longang JK, Gerstner F, Apel KS, Blanco-Redondo B, Sowoidnich L, Janzen E, Langenhan T, Wirth B, and Simon CM (2021). Central synaptopathy is the most conserved feature of motor circuit pathology across spinal muscular atrophy mouse models. iScience 24, 103376. 10.1016/j.isci.2021.103376. [PubMed: 34825141]
79. Simon CM, Dai Y, Van Alstyne M, Koutsioumpa C, Pagiazitis JG, Chalif JI, Wang X, Rabinowitz JE, Henderson CE, Pellizzoni L, and Mentis GZ (2017). Converging mechanisms of p53 activation drive motor neuron degeneration in spinal muscular atrophy. Cell Rep. 21, 3767–3780. 10.1016/j.celrep.2017.12.003. [PubMed: 29281826]
80. Chen Y, Wang B, Liu D, Li JJ, Xue Y, Sakata K, Zhu LQ, Heldt SA, Xu H, and Liao FF (2014). Hsp90 chaperone inhibitor 17-AAG attenuates Abeta-induced synaptic toxicity and memory impairment. J. Neurosci 34, 2464–2470. 10.1523/JNEUROSCI.0151-13.2014. [PubMed: 24523537]
81. Zuccato C, and Cattaneo E (2007). Role of brain-derived neurotrophic factor in Huntington's disease. Prog. Neurobiol 81, 294–330. 10.1016/j.pneurobio.2007.01.003. [PubMed: 17379385]
82. Heikkinen T, Lehtimäki K, Vartiainen N, Puoliväli J, Hendricks SJ, Glaser JR, Bradaia A, Wadel K, Touller C, Kontkanen O, et al. (2012). Characterization of neurophysiological and behavioral changes, MRI brain volumetry and 1H MRS in zQ175 knock-in mouse model of Huntington's disease. PLoS One 7, e50717. 10.1371/journal.pone.0050717. [PubMed: 23284644]
83. Keilani S, Chandwani S, Dolios G, Bogush A, Beck H, Hatzopoulos AK, Rao GN, Thomas EA, Wang R, and Ehrlich ME (2012). Egr-1 induces DARPP-32 expression in striatal medium spiny neurons via a conserved intragenic element. J. Neurosci 32, 6808–6818. 10.1523/JNEUROSCI.5448-11.2012. [PubMed: 22593050]

84. Herman AM, Khandelwal PJ, Stanczyk BB, Rebeck GW, and Moussa CEH (2011). β-amyloid triggers ALS-associated TDP-43 pathology in AD models. Brain Res. 1386, 191–199. 10.1016/j.brainres.2011.02.052. [PubMed: 21376022]

85. Rosenberger AFN, Morrema THJ, Gerritsen WH, van Haastert ES, Snkhchyan H, Hilhorst R, Rozemuller AJM, Scheltens P, van der Vies SM, and Hoozemans JJM (2016). Increased occurrence of protein kinase CK2 in astrocytes in Alzheimer's disease pathology. J. Neuroinflammation 13, 4. 10.1186/s12974-015-0470-x. [PubMed: 26732432]

86. Takahashi M, Ko LW, Kulathingal J, Jiang P, Sevlever D, and Yen SHC (2007). Oxidative stress-induced phosphorylation, degradation and aggregation of alpha-synuclein are linked to upregulated CK2 and cathepsin D. Eur. J. Neurosci 26, 863–874. 10.1111/j.1460-9568.2007.05736.X. [PubMed: 17714183]

87. Waxman EA, and Giasson BI (2011). Characterization of kinases involved in the phosphorylation of aggregated α-synuclein. J. Neurosci. Res 89, 231–247. 10.1002/jnr.22537. [PubMed: 21162130]

88. Masliah E, Iimoto DS, Mallory M, Albright T, Hansen L, and Saitoh T(1992). Casein kinase II alteration precedes tau accumulation in tangle formation. Am. J. Pathol 140, 263–268. [PubMed: 1739121]

89. Ekholm-Reed S, Goldberg MS, Schlossmacher MG, and Reed SI (2013). Parkin-dependent degradation of the F-box protein Fbw7β promotes neuronal survival in response to oxidative stress by stabilizing Mcl-1. Mol. Cell Biol 33, 3627–3643. 10.1128/MCB.00535-13. [PubMed: 23858059]

90. Li J, Pauley AM, Myers RL, Shuang R, Brashler JR, Yan R, Buhl AE, Ruble C, and Gurney ME (2002). SEL-10 interacts with presenilin 1, facilitates its ubiquitination, and alters A-beta peptide production. J. Neurochem 82, 1540–1548. 10.1046/j.1471-4159.2002.01105.x. [PubMed: 12354302]

91. Jacks T, Remington L, Williams BO, Schmitt EM, Halachmi S, Bronson RT, and Weinberg RA (1994). Tumor spectrum analysis in p53-mutant mice. Curr. Biol 4, 1–7. 10.1016/s0960-9822(00)00002-6. [PubMed: 7922305]

92. Tsunoda T, and Takagi T (1999). Estimating transcription factor bind-ability on DNA. Bioinformatics 15, 622–630. 10.1093/bioinformatics/15.7.622. [PubMed: 10487870]

93. Ippolito DM, and Eroglu C (2010). Quantifying synapses: an immunocytochemistry-based assay to quantify synapse number. J.Vis.Exp 16, 2270. 10.3791/2270.

Highlights

- PolyQ expansion in HTT exon 1 interferes with Mdm2 E3 ligase and stabilizes p53
- Stabilization of p53 in HD leads to the degradation of HSF1 transcription factor
- Degradation of HSF1 in HD increases HTT aggregation and striatal pathology
- $p53^{cKO}$ in MSNs in zQ175 mice restores HSF1 levels and HD-related phenotypes

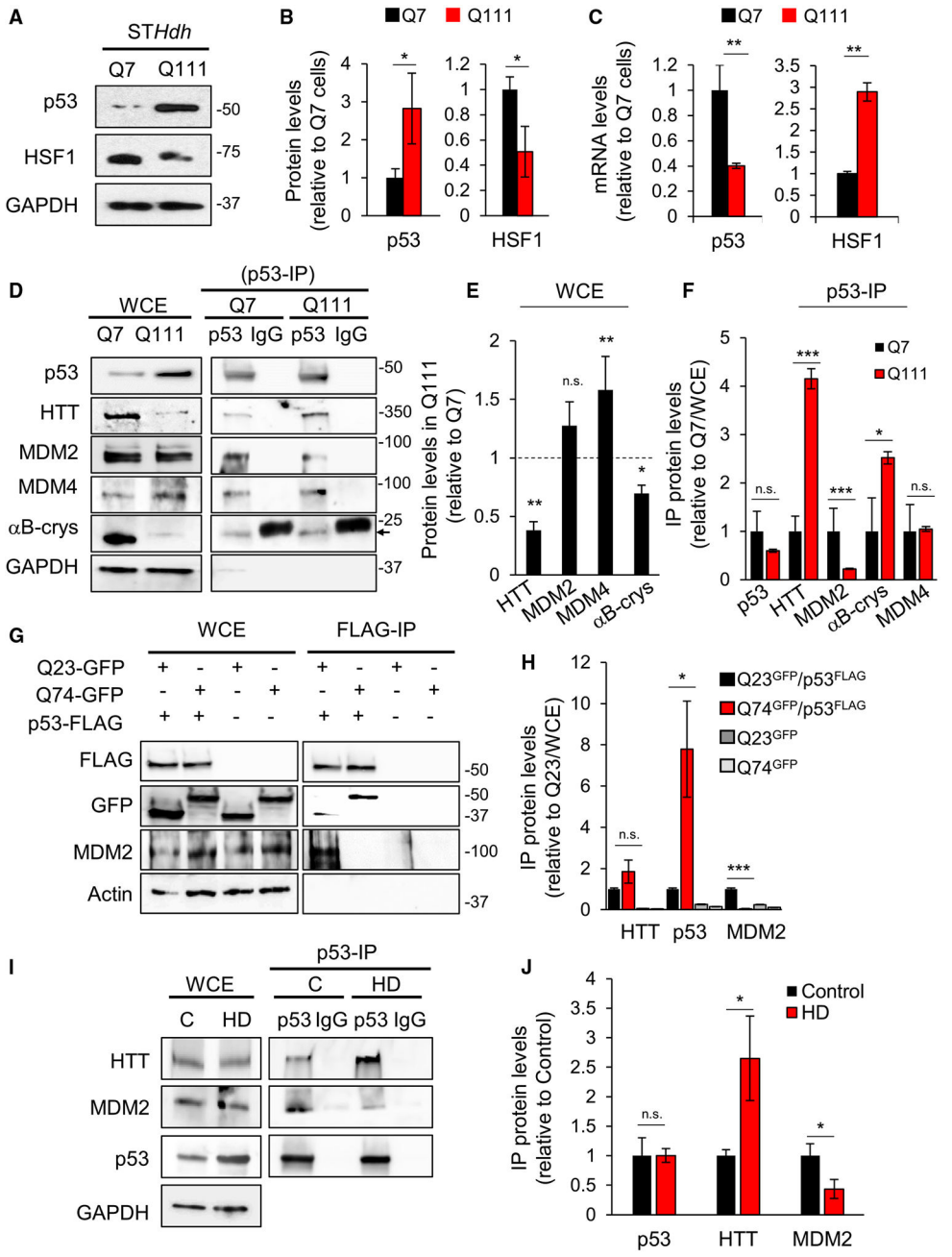

Figure 1. PolyQ-expanded HTT stabilizes p53 protein levels by interfering with p53-MDM2 interaction

(A and B) p53 and HSF1 protein levels in Q111 cells relative to Q7 (n = 5).

(C) p53 and HSF1 mRNA levels in Q111 cells relative to Q7 (n = 3).

(D) p53 immunoprecipitation (IP) in Q7 and Q111 cells using IgG as a negative control. GAPDH was used as a loading control of the whole-cell extract (WCE). Arrow points to pulled down αB-crys, unspecific bands in the IgG presented a higher molecular weight and were not considered in the analysis.

(E) HTT, MDM2, MDM4, and αB-crys protein levels in the WCE of Q111 relative to Q7 cells (n = 3).

(F) p53, HTT, MDM2, MDM4, and αB-crys protein levels pulled down by p53 in Q7 and Q111 cells. Data were normalized to total levels of each protein in the WCE and relativized to Q7 cells (n = 3).

(G) FLAG-IP in Q7 cells co-transfected with human HTT exon 1 containing Q23-GFP (non-pathogenic) or Q74-GFP (pathogenic) and human p53-FLAG.

(H) p53, HTT, and MDM2 protein levels pulled down by FLAG and relativized to Q23-expressing cells (n = 4).

(I) p53-IP in striatum samples from unaffected (control, C) and HD patients. IgG was used as a negative control.

(J) HTT, MDM2, and p53 protein levels pulled down by p53 or IgG and relativized to control (n = 3).

Error bars represent mean ± SEM. Unpaired t test; *p < 0.05, **p < 0.01, ***p < 0.001; not significant (n.s.). See also Figure S1 for supporting information and Data S1 for uncropped immunoblots.

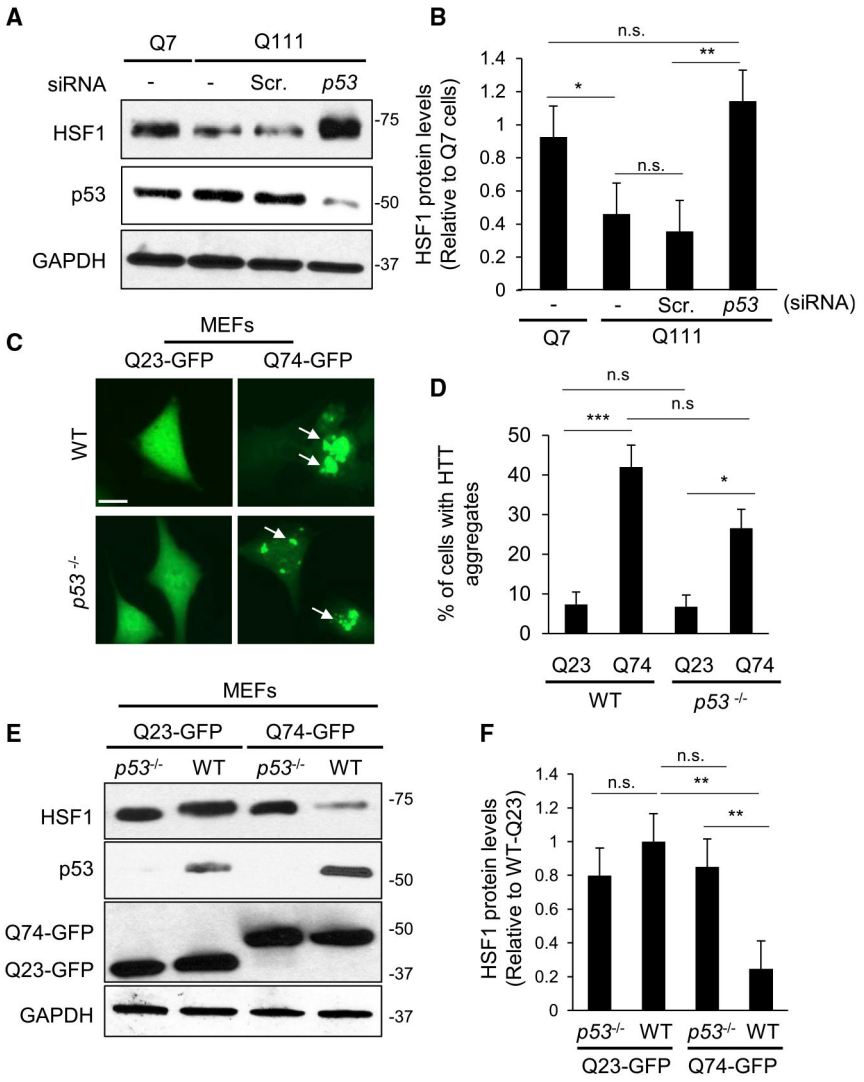

Figure 2. Stabilization of p53 in HD cell models is necessary for HSF1 pathological degradation

(A and B) HSF1 and p53 protein levels in Q7 and Q111 non-transfected cells (−) and Q111 treated cells with scramble (scr.) or si*p53* (n = 3).

(C) WT and *p53*$^{-/-}$ MEFs transfected with human HTT exon 1 Q23-GFP or Q74-GFP. Scale bar, 5 μm.

(D) Percent of WT and *p53*$^{-/-}$ MEFs cells containing GFP-HTT-Q74 aggregates (n = 200 cells, n = 3 experiments).

(E) Immunoblotting in WT and *p53*$^{-/-}$ MEFs transfected with human HTT exon 1 Q23-GFP or Q74-GFP.

(F) HSF1 protein levels from images in (E). Data were relativized to WT-Q23-expressing cells (n = 3).

Error bars represent mean ± SEM. One-way ANOVA with Tukey's post hoc test. *p < 0.05, **p < 0.01, ***p < 0.001; not significant (n.s.). See Data S1 for uncropped immunoblots.

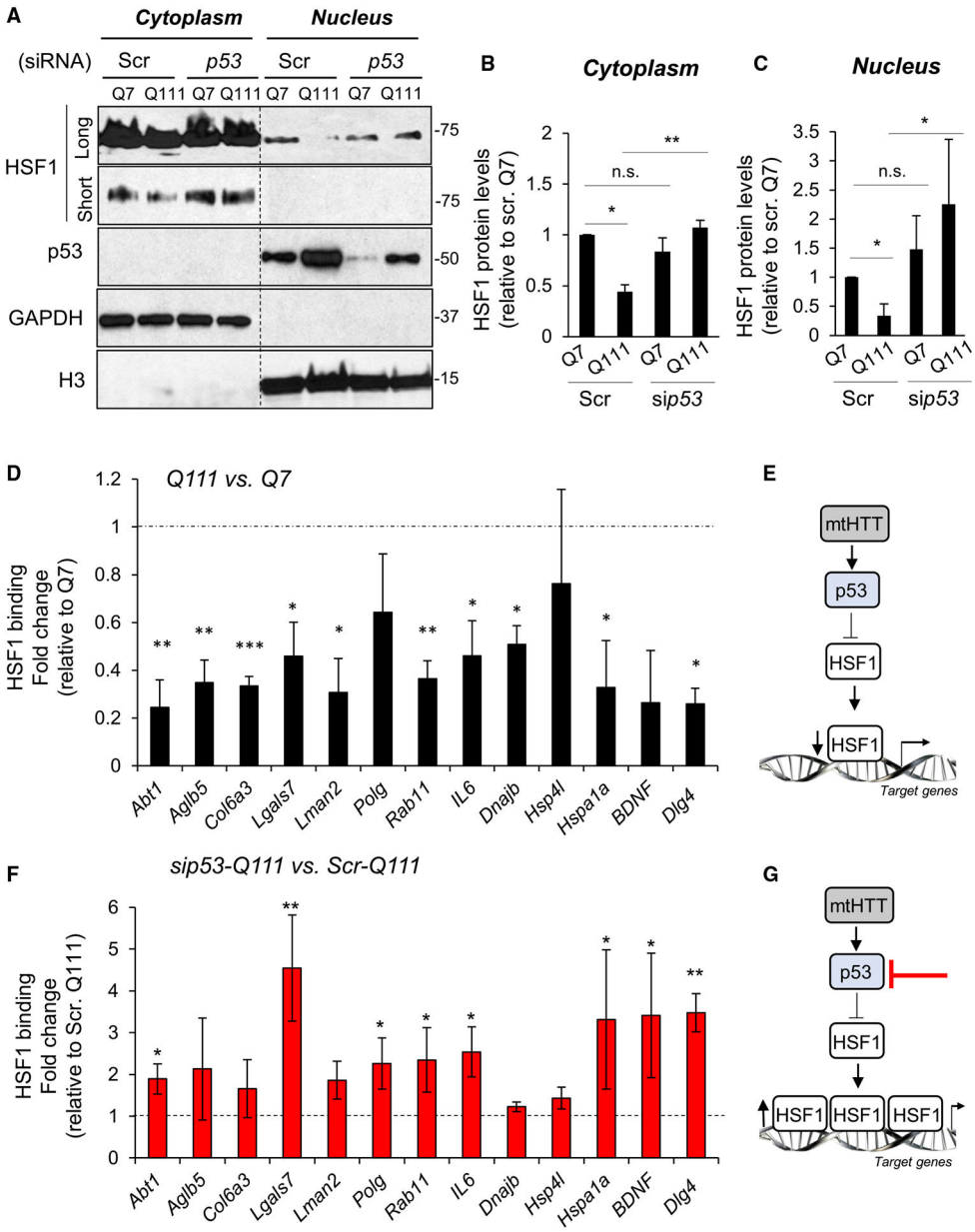

Figure 3. p53 depletion restores HSF1 nuclear accumulation and HSF1 DNA binding to target genes dysregulated in HD cells

(A) Immunoblotting in cytoplasm and nuclear fractions of Q7 and Q111 cells treated cells with scr. or si*p53*. HSF1 is shown at two different exposures (long and short).

(B and C) HSF1 protein levels in the cytoplasmic (B) and nuclear (C) fractions of Q111 relative to Q7 cells (n = 3).

(D) HSF1 ChIP in Q7 and Q111 cells on HSF1 gene targets shown by Riva et al.[31] (n = 3).

(E) Diagram showing the silencing effect of p53 on HSF1 DNA binding.

(F) HSF1 ChIP in Q111 cells treated with scr. or si*p53* (n = 3).

(G) Diagram showing the enhancing effect of silencing p53 on HSF1 DNA binding.

Error bars represent mean ± SEM. One-way ANOVA with Tukey's post hoc test (B and C), unpaired t test (D and F). *$p < 0.05$, **$p < 0.01$, ***$p < 0.001$; not significant (n.s.). See also Figure S2 for supporting information and Data S1 for uncropped immunoblots.

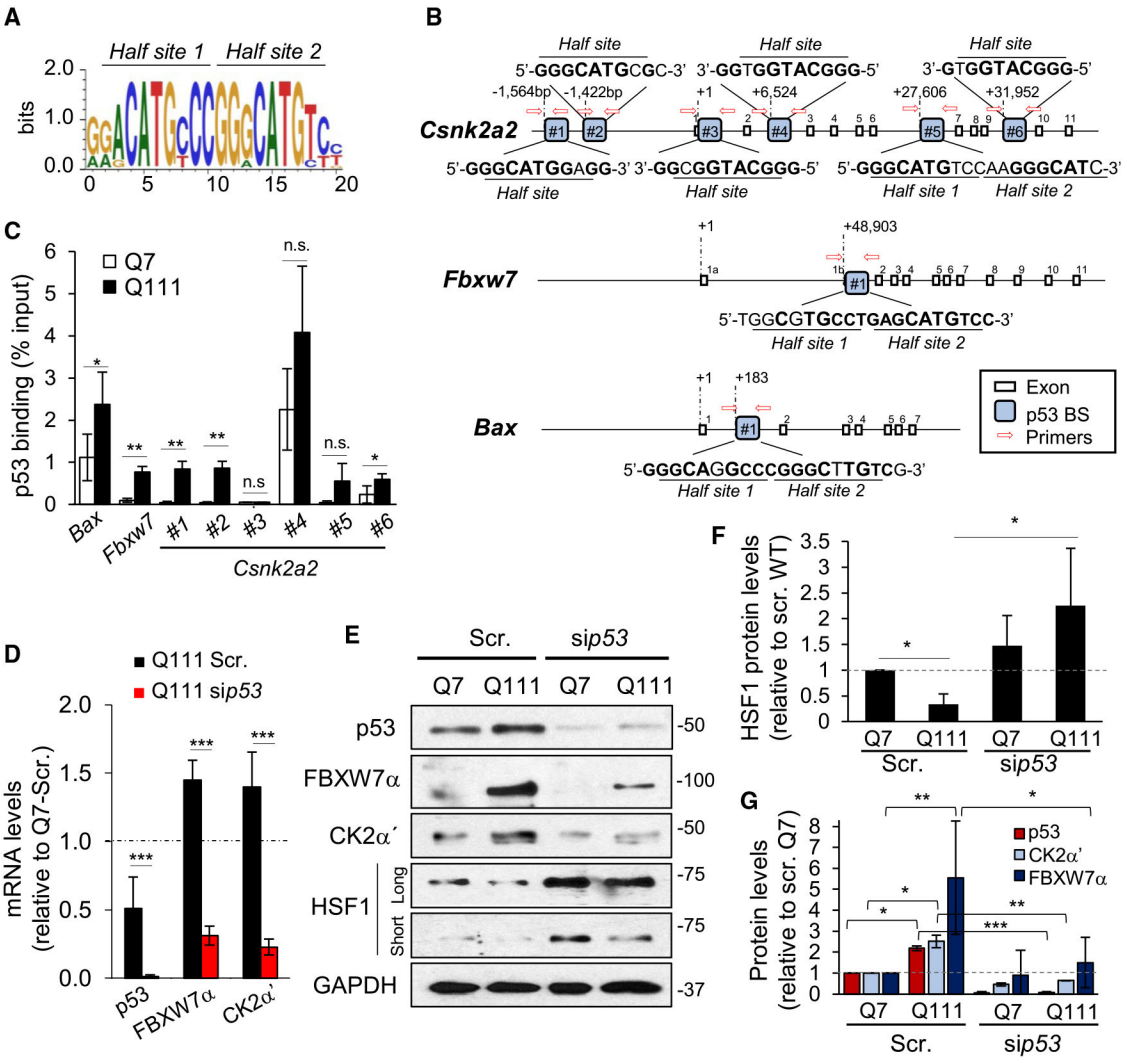

Figure 4. p53 regulates the transcriptional activation of components of the HSF1 degradation pathway

(A) Consensus p53 DNA-binding motif represented by Motif Express.

(B) Genomic mapping of p53 DNA-binding motifs in *Bax*,[40] *Fbxw7*, and *Csnk2a2* (CK2α′). Bolded base pairs are present in the consensus p53 DNA-binding motif.

(C) p53 ChIP in Q111 cells treated with scr. or sip53 (n = 6).

(D) p53, FBXW7α, and CK2α′ mRNA levels analyzed by qRT-PCR (n = 3).

(E) Immunoblotting in Q7 and Q111 cells treated cells with scr. or si*p53*. HSF1 is shown at a long and short exposure.

(F and G) (F) HSF1 and (G) p53, FBXW7α, and CK2α′ protein levels were quantified from images in (E) (n = 3).

Error bars represent mean ± SEM. One-way ANOVA with Tukey's post hoc test (D–G), unpaired t test (C). *p < 0.05, **p < 0.01, ***p < 0.001; not significant (n.s.). See also Figures S3 and S4 for supplemental information and Data S1 for uncropped immunoblots.

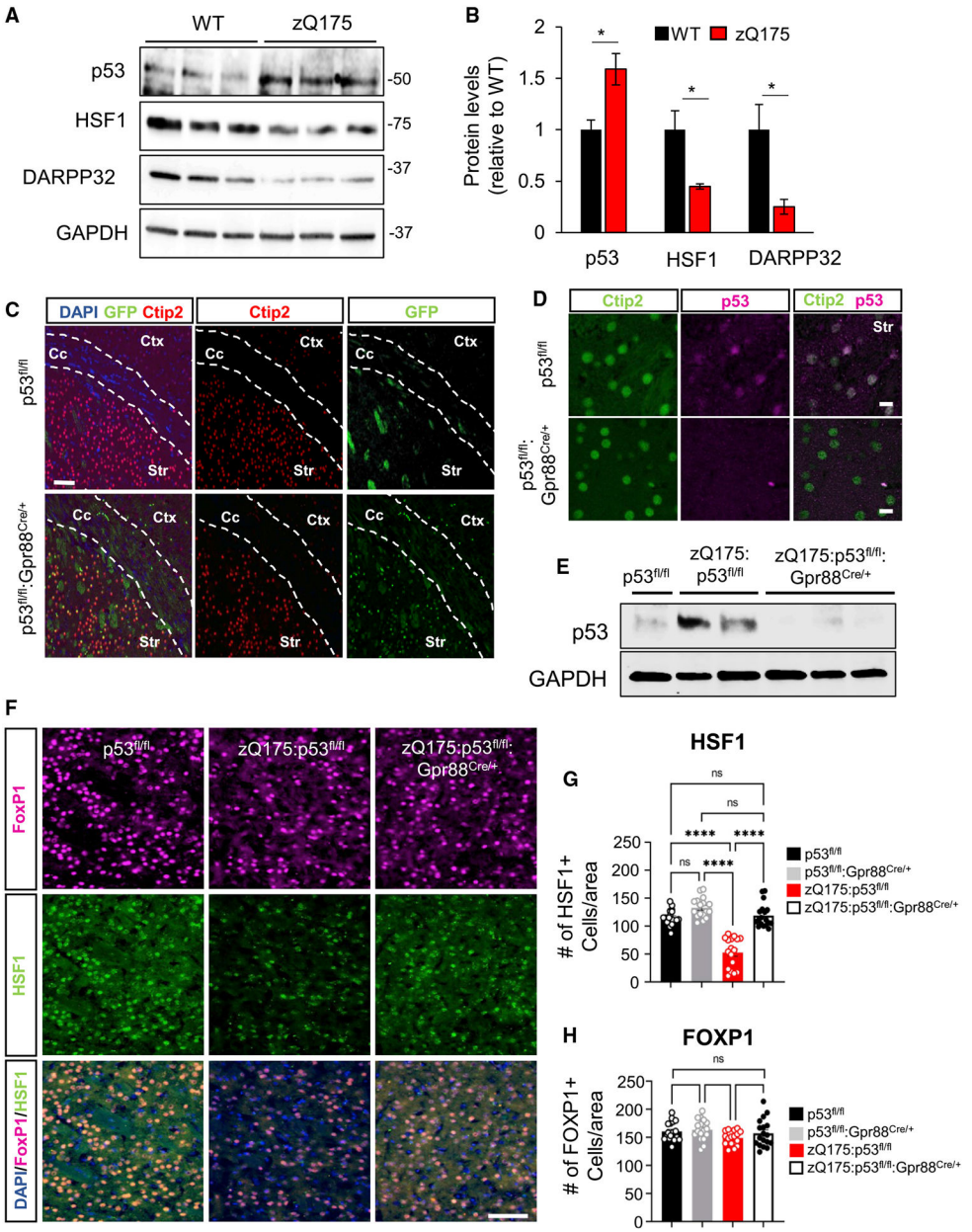

Figure 5. Conditional deletion of p53 in MSNs of the zQ175 prevented HSF1 protein degradation in MSNs

(A and B) p53, HSF1, and DARPP-32 protein levels in striatum samples from 12-month-old WT and zQ175 mice (n = 3).

(C) GFP and Ctip2 in the dorsal striatum (Str.), corpus callosum (C.c.), and cortex (Ctx) of 6 month-old $p53^{fl/fl}$ and $p53^{fl/fl}$:$Gpr88^{Cre/+}$ (n = 3).

(D) p53 immunostaining in striatum samples from 6-month-old WT ($p53^{+/+}$), $p53^{fl/fl}$, and $p53^{fl/fl}$:$Gpr88^{Cre/+}$ (n = 3 mice/genotype).

(E) p53 in the dorsal striatum of $p53^{fl/fl}$ and $p53^{fl/fl}$:$Gpr88^{Cre/+}$ (n = 3 mice/genotype).

(F) HSF1 and FOXP1 immunofluorescence in the dorsal striatum of $p53^{fl/fl}$, zQ175:$p53^{fl/fl}$, and zQ175:$p53^{fl/fl}$:$Gpr88^{Cre/+}$.

(G and H) Number of $HSF1^{+}$ (G) and $FoxP1^{+}$ cells (H) in the dorsal striatum of $p53^{fl/fl}$, zQ175:$p53^{fl/fl}$, and zQ175:$p53^{fl/fl}$:$Gpr88^{Cre/+}$ from representative images in (F) (n = 27 images from 3 different ROIs and 3 coronal brain slices spanning the striatum region and 3 mice/genotype).

Scale bars, 100 μm (C), 50 μm (E and F). Error bars represent SEM. One-way ANOVA with Tukey's post hoc test. *$p < 0.05$, **$p < 0.01$; not significant (n.s.). See also Figures S5 and S6 for supplemental information and Data S1 for uncropped immunoblots.

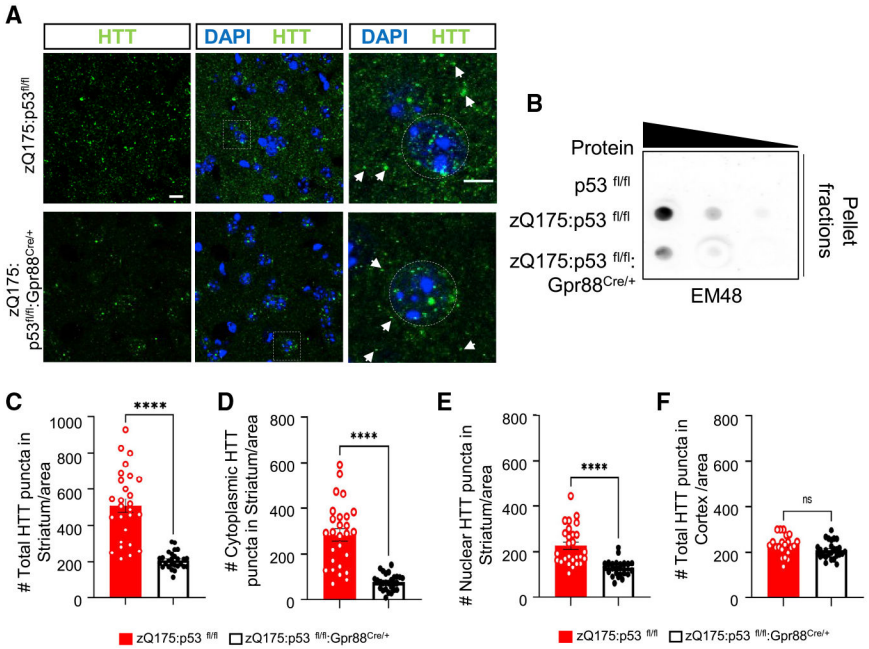

Figure 6. Conditional deletion of p53 in MSNs of the zQ175-ameliorated HTT aggregation in the striatum

(A) Representative images of HTT puncta (ab109115) in the dorsal striatum of zQ175:p53$^{fl/fl}$ and zQ175:p53$^{fl/fl}$:Gpr88$^{Cre/+}$ (n = 3 mice/genotype). Scale bar, 10 μm. The right panels represent an inlet of the left panels with nuclei surrounded by a circle. All mice were analyzed at age 6 months. Arrows indicate representative cytoplasmic puncta. DAPI stains nuclei

(B) HTT dot blot analysis in striatum pellet fractions solubilized with Urea 8M at different protein concentrations (5, 10, 20 μg).

(C) Total HTT puncta in 11.23 mm^2 area in the dorsal striatum of zQ175:p53$^{fl/fl}$ and zQ175:p53$^{fl/fl}$: Gpr88$^{Cre/+}$.

(D and E) Cytoplasmic (D) and nuclear (E) HTT puncta number per 11.23 mm^2 area in the dorsal striatum of zQ175:p53$^{fl/fl}$ and zQ175:p53$^{fl/fl}$: Gpr88$^{Cre/+}$.

(F) Total HTT puncta number in the cortex of zQ175:p53$^{fl/fl}$ and zQ175:p53$^{fl/fl}$:Gpr88$^{Cre/+}$. HTT puncta number was calculated using the Puncta Analyzer plugin from ImageJ (n = 27 images from 3 different ROIs and 3 coronal brain slices spanning the striatum region and 3 mice/genotype).

Error bars represent SEM. One-way ANOVA with Tukey's post hoc test. *p < 0.05, **p < 0.01; not significant (n.s.).

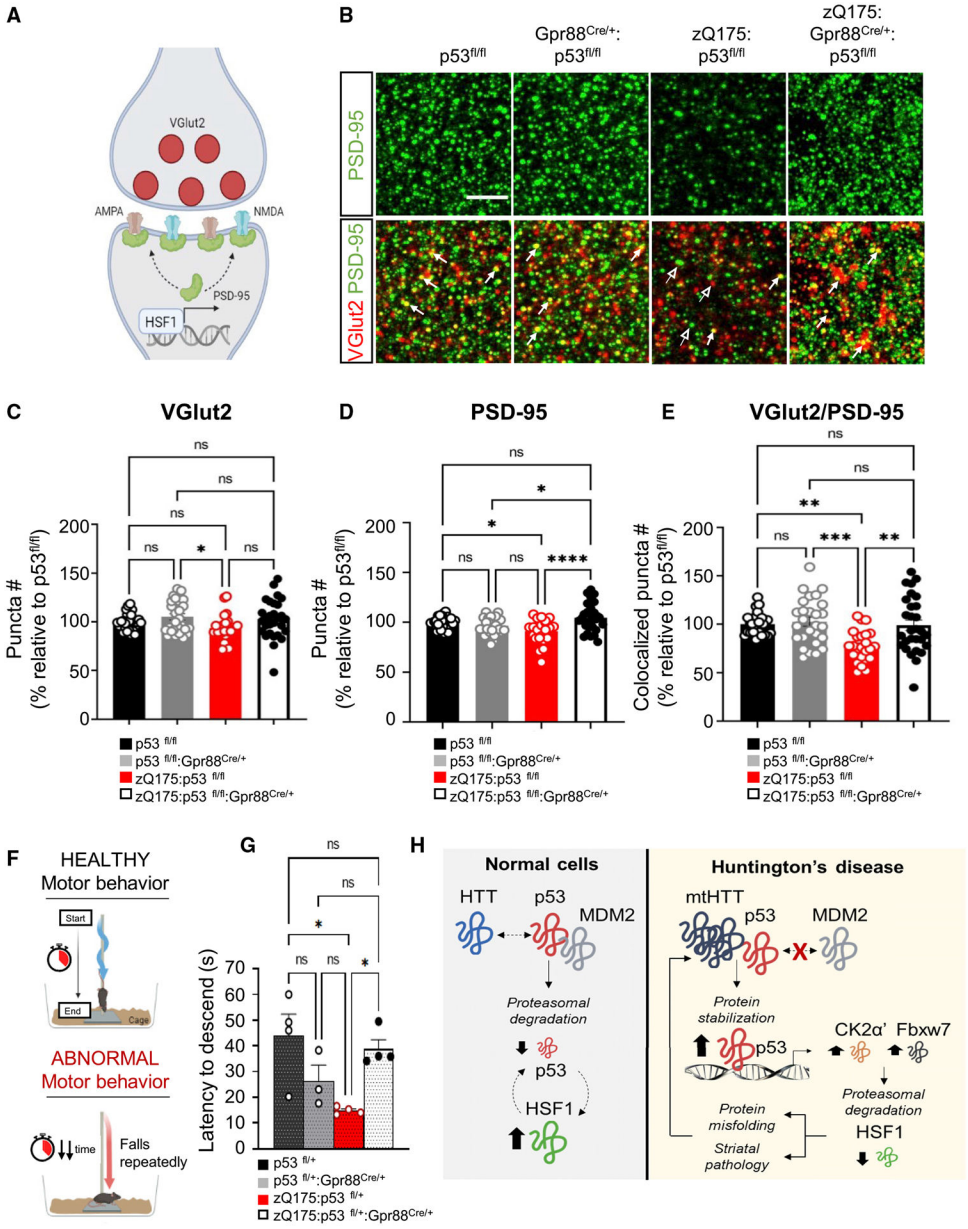

Figure 7. Synapse density loss in the dorsal striatum and motor deficits are ameliorated in zQ175 lacking p53 in MSNs

(A) Diagram of a T-S synapse showing PSD-95 (postsynaptic marker) and VGlut2 (presynaptic marker). Graphic was created with Biorender.com.

(B) VGlut2 and PSD-95 immunofluorescence in $p53^{fl/fl}$, $p53^{fl/fl}$:$Gpr88^{Cre/+}$, zQ175:$p53^{fl/fl}$, and zQ175:$p53^{fl/fl}$:$Gpr88^{Cre/+}$ mice. Images were edited and oversaturated to better illustrate the colocalization between VGlut2 and PSD-95 (see Figures S7A and S7B for representative unedited images). Scale bar, 5 μm. Closed arrows indicate VGlut2/PSD-95 colocalization, open arrows indicate non-colocalizing puncta.

(C–E) Puncta number for VGlut2 (C), PSD-95 (D), and colocalization VGlut2/PSD-95 (E) was calculated from unedited immunofluorescence images (n = 27 slices from 3 coronal

brain slices spanning the striatum region, each slice containing a z stack of 15 images, 3 mice/genotype).

(F) Latency to descend pole in 6-month-old $p53^{fl/+}$, $p53^{fl/+}$:$Gpr88^{Cre/+}$, zQ175:$p53^{fl/+}$, and zQ175: $p53^{fl/+}$:$Gpr88^{Cre/+}$ mice (n = 3–5 mice/group). The right panel represents expected outcomes for “healthy” and “abnormal” motor behavior.

(G) Summary schematic for the mechanistic connection between mtHTT, p53, and HSF1 in HD.

Error bars represent mean ± SEM. One-way ANOVA with Tukey’s post hoc test. *p < 0.05, **p < 0.01, ***p < 0.001, ****p < 0.0001; not significant (n.s.). See also Figurse S7C and S7D for supporting information.

KEY RESOURCES TABLE

REAGENT or RESOURCE	SOURCE	IDENTIFIER
Antibodies		
Rabbit anti-CK2α′	Novus	Cat#NB100-379; RRID:AB_10000080
Rabbit anti-CK2α′	Proteintech	Cat#10606-1-AP; RRID:AB_2292447
Mouse anti-HTT (EM48)	Millipore	Cat#MAB5374; RRID:AB_10055116
Rabbit anti-HTT	Abcam	Cat#ab109115; RRID:AB_10863082
Rabbit anti-HSF1	Bethyl	Cat#A303-176A; RRID:AB_10892628
Mouse anti-p53 (DO-1)	Santa Cruz	Cat#sc-126; RRID: AB_628082
Rabbit anti-p53 (FL-393)	Santa Cruz	Cat#sc-6243; RRID:AB_653753
Mouse anti-MDM2	Santa Cruz	Cat#sc-965; RRID:AB_627920
Rabbit anti-MDM4	Aviva Systems Biology	Cat#AVARP06007_T100; RRID:AB_841544
Rabbit anti-aB-crys	Enzo	Cat#ADI-SPA-223D; RRID:AB_2039025
Rabbit anti-FBXW7	Abcam	Cat#ab109617; RRID:AB_2687519
Mouse anti-GAPDH	Santa Cruz	Cat#sc-365062; RRID:AB_10847862
Mouse anti-actin	Santa Cruz	Cat#sc-8432; RRID:AB_626630
Rabbit anti-H3	Cell Signaling Technology	Cat#9715; RRID:AB_331563
Mouse anti-FLAG	Santa Cruz	Cat#sc-166355; RRID:AB_2017593
Mouse anti-GFP	Santa Cruz	Cat#sc-9996; RRID:AB_627695
Rabbit anti-IgG	R&D Systems	Cat#AF008; RRID:AB_354521
Mouse anti-IgG	R&D Systems	Cat#AF007; RRID:AB_354520
Rat anti-CTIP2	Abcam	Cat#ab18465; RRID:AB_2064130
Rat anti-DARPP-32	R&D Systems	Cat#MAB4230; RRID:AB_2169021
Rat anti-HSF1	Enzo	Cat#ADI-SPA-950F; RRID:AB_11181482
Mouse anti-p53	Novus Biologicals	Cat#NB200-10355; RRID:AB_10001083
Mouse anti-FOXP1	Abcam	Cat#ab32010; RRID:AB_1141518
Rabbit anti-Cre	Cell Signaling Technology	Cat#15036S; RRID:AB_2798694
Rabbit anti-PSD-95	Thermo Fisher	Cat#51-6900; RRID:AB_2533914
Guinea pig anti-VGLUT2	Millipore	Cat#AB2251-I; RRID:AB_2665454
Goat anti-rabbit Alexa 488	Invitrogen	Cat#A-11008; RRID:AB_10563748
Goat anti-rat Alexa 488	Invitrogen	Cat#A-11006; RRID:AB_141373
Goat anti-mouse Alexa 488	Invitrogen	Cat#A-11001; RRID:AB_2534069
Goat anti-guinea pig 488	Invitrogen	Cat#A-11073; RRID:AB_2534117
Goat anti-rabbit Alexa 594	Invitrogen	Cat#A-11012; RRID:AB_2534079
Goat anti-rat Alexa 594	Invitrogen	Cat#A-11007; RRID:AB_10561522
Goat anti-mouse Alexa 594	Invitrogen	Cat#A-11005; RRID:AB_2534073
Goat anti-rat Alexa 647	Invitrogen	Cat#A-21247; RRID:AB_141778
Goat anti-mouse Alexa 647	Invitrogen	Cat#A-21235; RRID:AB_2535804
Biological samples		
Human Striatum Control (C1c)	Harvard Brain Tissue Resource Center	AN10805

REAGENT or RESOURCE	SOURCE	IDENTIFIER
Human Striatum HD (H1c)	Harvard Brain Tissue Resource Center	AN08979
Human Striatum Control (C2c)	Harvard Brain Tissue Resource Center	AN00559
Human Striatum HD (H2c)	Harvard Brain Tissue Resource Center	AN10878
Human Striatum Control (C4c)	Harvard Brain Tissue Resource Center	AN04642
Human Striatum HD (H4c)	Harvard Brain Tissue Resource Center	AN18418
Chemicals, peptides, and recombinant proteins		
Dulbecco's modified Eagle's medium (DMEM)	Genesee	Cat#25-500
SYBR mix	Roche	Cat#4707516001
Lipofectamine LTX Reagent	Invitrogen	Cat#15338100
Critical commercial assays		
EZview Red Anti-FLAG M2 affinity gel	Millipore Sigma	Cat# F2426
MiniElute PCR Purification Kit	Qiagen	Cat# 28004
RNeasy extraction kit	Qiagen	Cat#74104
Superscript First Strand Synthesis System	Invitrogen	Cat#11904018
NE-PER Extraction Kit	Thermofisher	Cat#78833
TransAM p53 Transcription Factor ELISA Kit	Active Motif	Cat#41196
Experimental models: Cell lines		
mouse: striatal cells: STHdh$^{Q7/Q7}$	Coriell Cell Repositories	RRID:CVCL_M590
mouse: striatal cells: STHdh$^{Q111/Q111}$	Coriell Cell Repositories	RRID:CVCL_M591
mouse: p53$^{-/-}$ Kras G12D MEFs	Laboratory of David Kirsch, Duke University	N/A
Experimental models: Organisms/strains		
mouse: zQ175: B6J.129S1-*Htttm1Mfc*/190ChdiJ	The Jackson Laboratory	RRID:IMSR_JAX:027410
mouse: p53$^{fl/fl}$ mice: B6.129P2-*Trp53*^{tm1Brn}/J	Laboratory of Michael Lee, University of Minnesota	RRID:IMSR_JAX:008462
mouse: p53$^{-/-}$ mice: B6; 129S2-*Trp53*^{tm1Tyj}/J	Jacks et al., 1994[91]	RRID:IMSR_JAX:008462
mouse:Gpr88$^{Cre/+}$:Gpr88$^{tm1.1(cre/GFP)Rpa}$	The Jackson Laboratory	RRID: MGI:6201721
mouse: HSF1$^{-/-}$ mice: B6N(Cg)-Hsf1$^{tm1(KOMP)Vlcg}$/JMmucd	Mutant Mouse Resource and Research Center	Stock No. 048101-UCD
mouse: CMV-CRE mice: B6.C-Tg(CMV-cre)1Cgn/J	Mouse Genetics laboratory, University of Minnesota	RRID:IMSR_JAX:006,054
Oligonucleotides		
FlexiTube siRNA	Qiagen	Cat#1027417
ON-TARGETplus control Non-targeting pool siRNA	Dharmacon	Cat#D-001810-10
See Table S2 for primer sequences	IDT Integrated technologies	N/A
Recombinant DNA		
HTT exon 1 Q23-GFP	Addgene	RRID:Addgene_40261
HTT exon 1 Q74-GFP	Addgene	RRID:Addgene_40262
p53-FLAG	Addgene	RRID:Addgene_10838
HTT full length Q23-FLAG	Addgene	RRID:Addgene_111723

REAGENT or RESOURCE	SOURCE	IDENTIFIER
HTT full length Q54-FLAG	Addgene	RRID:Addgene_111727
p53-GFP	Addgene	RRID:Addgene_11770
Software and algorithms		
ImageJ		https://imagej.nih.gov/ij/index.html
p53 binding site identification	Tsunoda & Takagi, 1999[92]	https://tfbind.hgc.jp/
PunctaAnalyzer ImageJ	Ippolito & Eroglu, 2010[93]	N/A
Prism 8 software	GraphPad, San Diego, CA	https://www.graphpad.com/scientific-software/prism/
Excel software	Microsoft	https://www.microsoft.com/en-us/microsoft-365/excel